*Human Molecular Genetics*, 2021, Vol. 30, No. 14 1305–1320

https://doi.org/10.1093/hmg/ddab112
Advance Access Publication Date: 28 April 2021
General Article

GENERAL ARTICLE

# Acute and chronic *tirasemtiv* treatment improves *in vivo* and *in vitro* muscle performance in actin-based nemaline myopathy mice

Josine M. de Winter[1,†], Charlotte Gineste[2,†], Elisa Minardi[3,†], Lorenza Brocca[3], Maira Rossi[3], Tamara Borsboom[1], Alan H. Beggs[4], Monique Bernard[2], David Bendahan[2], Darren T. Hwee[5], Fady I. Malik[5], Maria Antonietta Pellegrino[3,6], Roberto Bottinelli[3,7,†], Julien Gondin[2,8,†] and Coen A.C. Ottenheijm[1,†,*]

[1]Department of Physiology, Amsterdam UMC (location VUmc), Amsterdam 1081 HV, The Netherlands, [2]Aix-Marseille Univ, CNRS, CRMBM, UMR 7339, 13005 Marseille, France, [3]Department of Molecular Medicine, University of Pavia, Pavia 27100, Italy, [4]Division of Genetics and Genomics, The Manton Center for Orphan Disease Research, Boston Children's Hospital, Harvard Medical School, Boston, MA 02115, USA, [5]Research and Early Development, Cytokinetics Inc., South San Francisco, CA 94080, USA, [6]Interdipartimental Centre for Biology and Sport Medicine, University of Pavia, Pavia 27100, Italy, [7]Istituti Clinici Maugeri (IRCCS), Scientific Institute of Pavia, Pavia 27100, Italy and [8]Institut NeuroMyoGène, Université Claude Bernard Lyon 1, CNRS 5310, INSERM U1217, 69008, Lyon, France

*To whom correspondence should be addressed. Tel: +31 (0)20 444 8111; Email: c.ottenheijm@amsterdamumc.nl

## Abstract

Nemaline myopathy, a disease of the actin-based thin filament, is one of the most frequent congenital myopathies. To date, no specific therapy is available to treat muscle weakness in nemaline myopathy. We tested the ability of *tirasemtiv*, a fast skeletal troponin activator that targets the thin filament, to augment muscle force—both *in vivo* and *in vitro*—in a nemaline myopathy mouse model with a mutation (H40Y) in *Acta1*. In *Acta1*$^{H40Y}$ mice, treatment with *tirasemtiv* increased the force response of muscles to submaximal stimulation frequencies. This resulted in a reduced energetic cost of force generation, which increases the force production during a fatigue protocol. The inotropic effects of *tirasemtiv* were present in locomotor muscles and, albeit to a lesser extent, in respiratory muscles, and they persisted during chronic treatment, an important finding as respiratory failure is the main cause of death in patients with congenital myopathy. Finally, translational studies on permeabilized muscle fibers isolated from a biopsy of a patient with the *ACTA1*$^{H40Y}$ mutation revealed that at physiological $Ca^{2+}$ concentrations, *tirasemtiv* increased force generation to values that were close to those generated in muscle fibers of healthy subjects. These findings indicate the therapeutic potential of fast skeletal muscle troponin activators to improve muscle function in nemaline myopathy due to the *ACTA1*$^{H40Y}$ mutation, and future studies should assess their merit for other forms of nemaline myopathy and for other congenital myopathies.

[†]These authors contributed equally.

**Received:** December 21, 2020. **Revised:** March 9, 2021. **Accepted:** April 7, 2021

## Introduction

Congenital myopathies are a genetically heterogeneous group of early onset neuromuscular disorders characterized by distinct structural abnormalities in muscle fibers and by contractile weakness (1). The majority of these disorders are caused by defects either in the process of excitation–contraction coupling or in the assembly and interaction of proteins that make up the sarcomeres, the smallest contractile units in muscle. To date, no therapy is available to treat muscle weakness in congenital myopathies.

One of the most frequent congenital myopathies is nemaline myopathy (NEM; incidence ∼1:50 000 (2,3)). Currently, 12 genes have been implicated in NEM: alpha-actin 1 (*ACTA1*) (4), alpha- and beta-tropomyosin (*TPM3* and *TPM2*) (5,6), nebulin (*NEB*) (7), leiomodin-3 (*LMOD3*) (8), troponin T (*TNNT1* (9) and *TNNT3*) (10), cofilin 2 (*CFL2*) (11), myopalladin (*MYPN*) (12), kelch family members 40 (*KLHL40*) and −41 (*KLHL41*) (13,14), and kelch repeat and BTB (POZ) domain containing 13 (*KBTBD13*) (15). All of these genes encode proteins that are associated with the actin-based thin filament. Recent studies revealed that thin filament dysfunction is a major contributor to muscle weakness in NEM patients (16–23). Thus, thin-filament dysfunction is a therapeutic target in NEM.

Here, we aimed to test the ability of the small molecule, fast skeletal muscle troponin activator, *tirasemtiv*, to augment thin filament function in NEM. *Tirasemtiv* amplifies the response of the thin filament to calcium ($Ca^{2+}$) in fast skeletal muscle fibers, leading to increased muscle force at submaximal rates of nerve stimulation (24). Thus, troponin activation is an appealing therapeutic approach in NEM. In our studies, we took advantage of an NEM mouse model with the heterozygous NM_009606.3(Acta1):p.His42Tyr mutation in *Acta1* (25), one of the most frequently affected genes in NEM patients. Note that throughout the manuscript, this mutation is referred to as $Acta1^{H40Y}$ to be consistent with existing literature utilizing an older numbering scheme. We studied the acute and chronic *in vitro* and *in vivo* effects of *tirasemtiv* on skeletal muscle contractility and metabolism that included respiratory muscle, as respiratory failure is the main cause of death in NEM (1).

We found that acute and chronic treatment with *tirasemtiv* resulted in a profound increase in the force response to submaximal stimulation frequencies in $Acta1^{H40Y}$ mice. The energetic cost of force generation was reduced in muscle of *tirasemtiv*-treated $Acta1^{H40Y}$ mice. An interesting finding was that chronic treatment of $Acta1^{H40Y}$ mice with *tirasemtiv* also increased the force response to *maximal* stimulation, with no muscle mass increase. This suggests that muscle remodeling had occurred to improve contractility. Finally, studies on permeabilized muscle fibers isolated from a biopsy of a patient with the $ACTA1^{H40Y}$ mutation revealed that at physiological $Ca^{2+}$ concentrations, *tirasemtiv* increased force generation to values that were close to those generated in muscle fibers of healthy subjects. Together, these findings indicate the therapeutic potential of fast skeletal troponin activators to alleviate muscle weakness in NEM.

## Results

### Baseline characteristics of the mouse model

$Acta1^{H40Y}$ mice had lower body weights and lower muscle mass, except for the *soleus* muscle which had significantly increased muscle weight (Fig. 1A). According to previous studies (24), *tirasemtiv* specifically affects the contractility of fast-twitch muscle fibers with fast skeletal muscle troponin, which express type 2 MHC isoforms. Therefore, we evaluated the MHC isoform composition of EDL and *gastrocnemius* muscles, the muscles selected for our contractility assays. As shown in Figure 1B, both EDL and *gastrocnemius* muscles contain mainly type 2B MHC isoforms, with EDL muscle also significant amounts of type 2X MHC isoforms. Minor differences in MHC isoform proportions were observed between *Acta1*(WT) and $Acta1^{H40Y}$ mice. The magnitude of the effect of *tirasemtiv* by type 2 MHC isoform is unknown. Therefore, we isolated permeabilized single muscle fibers from a WT mouse muscle, determined their calcium sensitivity of force in the presence and absence of *tirasemtiv*, and determined the MHC isoform in the fibers. As shown in Figure 1C, *tirasemtiv* increased the calcium sensitivity of force with a comparable magnitude in both type 2AX and 2B fibers (with, as expected, no effect in type 1 fibers). Thus, both EDL and *gastrocnemius* muscles are appropriate for testing the efficacy of *tirasemtiv* to improve muscle function in the $Acta1^{H40Y}$ mouse model. Further characterization of both muscles showed that the cross-sectional area (CSA) of individual muscle fibers was smaller in EDL and *gastrocnemius* of $Acta1^{H40Y}$ mice compared to WT mice (Fig. 1D). Similarly, the maximal force generating capacity was lower in EDL and *gastrocnemius* of $Acta1^{H40Y}$ mice compared to WT mice (Fig. 1E).

Thus, EDL and *gastrocnemius* muscles of $Acta1^{H40Y}$ mice display contractile weakness. Both muscle types contain a high proportion of fast-twitch muscle fibers, providing a large treatment window for testing the efficacy of acute and chronic *tirasemtiv* administration.

### Effect of acute *tirasemtiv* administration

First, we evaluated the effect of acute administration of 3 μM *tirasemtiv* on the *in vitro* contractility of EDL muscle in 9-month-old *Acta1*(WT) and $Acta1^{H40Y}$ mice. This concentration was selected based on previous studies showing a maximal effect on contractility at 3 μM (without significantly slowing the rate of muscle relaxation) (26). *Tirasemtiv* induced a leftward shift of the force-stimulation frequency curve in both *Acta1*(WT) and $Acta1^{H40Y}$ EDL muscle (Fig. 2A, left panels). Consequently, the force generated at 40 Hz (normalized to maximal force at 200 Hz) increased by ∼50% in *Acta1*(WT) muscle and by ∼100% in $Acta1^{H40Y}$ mice (Fig. 2A, middle panels). *Tirasemtiv* did not affect the maximal force generated by EDL muscle (Fig. 2A, right panels). Absolute force values are shown in Table 1.

Second, we evaluated the effect of acute administration of 3 mg/kg *tirasemtiv* on the *in vivo* contractility of *gastrocnemius* muscle in 9-month-old mice. This treatment resulted in comparable *tirasemtiv* plasma concentrations in *Acta1*(WT) and $Acta1^{H40Y}$ mice (*Acta1*(WT): 11.7 ± 1.1 μM; $Acta1^{H40Y}$: 9.8 ± 0.9 μM; assessed nocturnally, the time of day at which the contractility experiments were performed). *Tirasemtiv* increased the force generated at 20 Hz (normalized to maximal force at 150 Hz) by ∼20% in *Acta1*(WT) muscle and by ∼26% in $Acta1^{H40Y}$ mice (Fig. 2B, left panels). *Tirasemtiv* did not affect the maximal force generated by *gastrocnemius* muscle (Fig. 2B, right panels). Absolute force values are shown in Table 2.

Thus, these findings show that acute administration of *tirasemtiv* increased *in vitro* and *in vivo* submaximal force generation of $Acta1^{H40Y}$ EDL and *gastrocnemius* mouse muscles.

### Effect of chronic *tirasemtiv* administration

Five-month-old *Acta1*(WT) and $Acta1^{H40Y}$ mice were fed chow enriched with *tirasemtiv* for 4 weeks. This treatment resulted

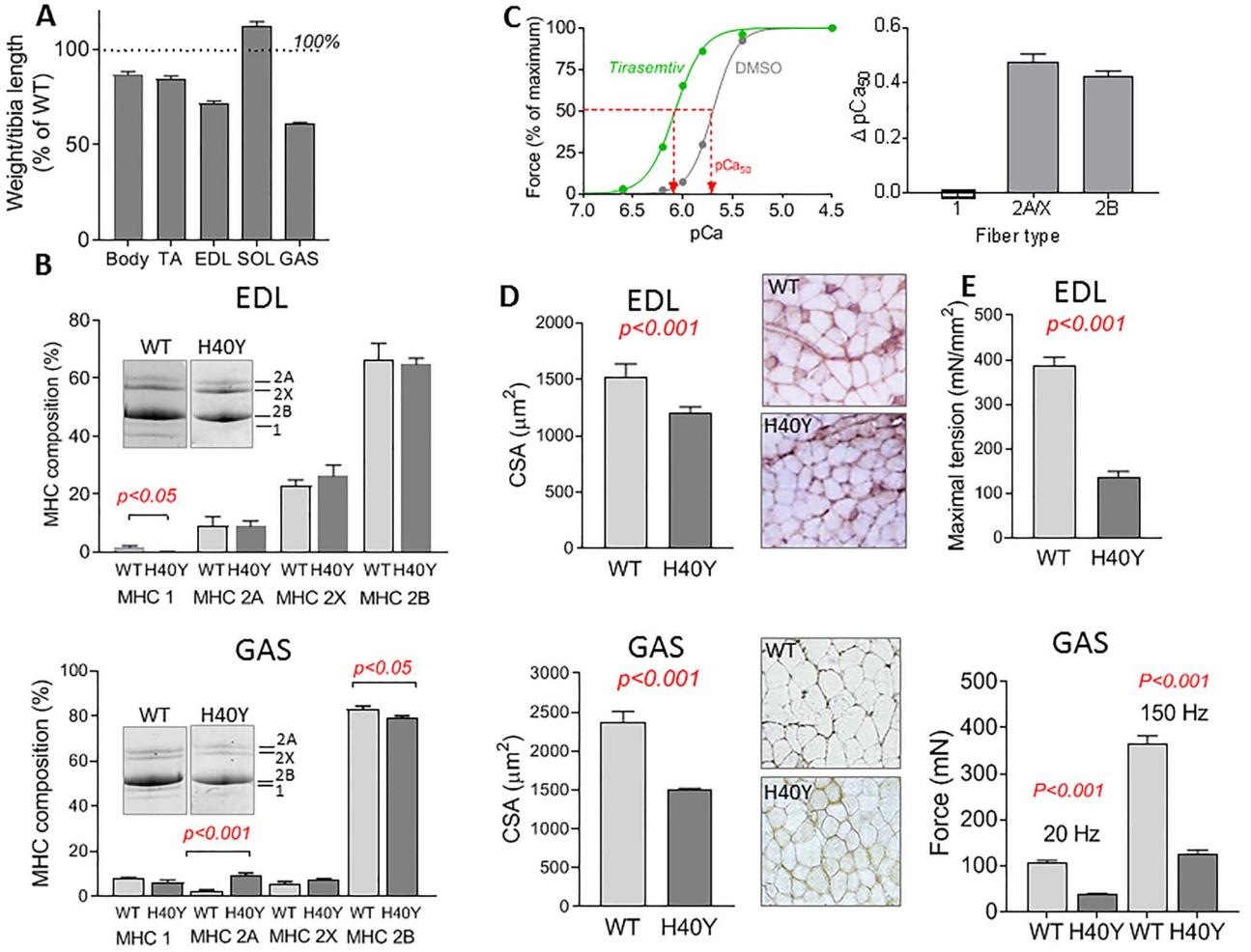


**Figure 1.** Characterization of the *Acta1*$^{H40Y}$ mouse model. (**A**) Body and wet muscle weights, normalized over tibia length. (**B**) MHC isoform composition of *extensor digitorum longus* (EDL, top) and *gastrocnemius* (GAS, bottom) muscles. (**C**) The effect of 10 μM *tirasemtiv* on the calcium sensitivity of force of single muscle fibers of EDL. Left panel shows a typical example of the effect of *tirasemtiv* on the force-pCa relation of a type 2B muscle fiber before exposure to *tirasemtiv* and during exposure to *tirasemtiv*. Right panel shows the results per fiber type. (**D**) Fiber CSA of EDL (top) and *gastrocnemius* (bottom) muscle. Right panels show representative cryosections stained with wheat germ agglutinin to demarcate muscle fibers. (**E**) Top: the maximal tension (*in vitro* force normalized to muscle CSA at 200 Hz stimulation) of EDL muscle. Bottom: the *in vivo* maximal force of *gastrocnemius* muscle at 20 and 150 Hz stimulation.

in comparable *tirasemtiv* plasma concentrations in *Acta1*(WT) and *Acta1*$^{H40Y}$ mice (*Acta1*(WT): 29 ± 4 μM; *Acta1*$^{H40Y}$: 22 ± 3 μM; assessed nocturnally, the time of day at which the contractility experiments were performed). After 4 weeks, no effect of *tirasemtiv* on muscle mass was observed in *Acta1*(WT) and in *Acta1*$^{H40Y}$ mice (Fig. 3A). In line with this finding, no effect of chronic *tirasemtiv* administration on fiber CSA in *gastrocnemius* muscle was observed (Fig. 3B). Furthermore, chronic *tirasemtiv* administration did not affect the proportion of fast-twitch muscle fibers (Fig. 3C), an important finding as this indicates that the number of fibers sensitive to *tirasemtiv* was not affected by chronic administration.

First, we evaluated the effect of chronic administration of *tirasemtiv* on the *in vitro* contractility of EDL of *Acta1*(WT) and *Acta1*$^{H40Y}$ mice. Note that after excision of the muscles from the mouse leg and prior to the contractility assay, muscles were bathed for ∼20 min in *tirasemtiv*-free Ringer solution. Previous work indicated that this time-frame is sufficient to completely remove *tirasemtiv* from the muscles. Interestingly, despite the removal of *tirasemtiv*, the chronic administration of *tirasemtiv* induced a small, but significant leftward shift of the force-stimulation frequency curve in both *Acta1*(WT) and *Acta1*$^{H40Y}$ EDL muscle (Fig. 4A, left panel). However, *post-hoc* analysis showed that the force generated at 40 Hz (normalized to maximal force at 200 Hz) was not significantly different between *tirasemtiv*-treated and vehicle-treated *Acta1*(WT) mice (Fig. 4A, middle panel). Note that the absolute force at 40 Hz was higher in *tirasemtiv*-treated than in vehicle-treated *Acta1*(WT) mice (Table 3). The *Acta1*$^{H40Y}$ mice had a similar response (Fig. 4A, left and middle panels). Interestingly, chronic administration of *tirasemtiv* significantly increased the maximal force generated by EDL muscle by ∼15% in *Acta1*(WT) mice and by ∼43% in *Acta1*$^{H40Y}$ mice (Fig. 4A, right panels). Absolute force values are shown in Table 3.

Next, we evaluated the effect of chronic administration of *tirasemtiv* on the *in vivo* contractility of *gastrocnemius* muscle in *Acta1*$^{H40Y}$ mice. Note that during these *in vivo* assays, *tirasemtiv* was present in the muscles. After 4 weeks, *Tirasemtiv* increased the force generated at 20 Hz (normalized to maximal force at 150 Hz) by ∼25% in *Acta1*$^{H40Y}$ muscle (Fig. 4B, top panel). *Tirasemtiv* also increased the maximal force (normalized to muscle

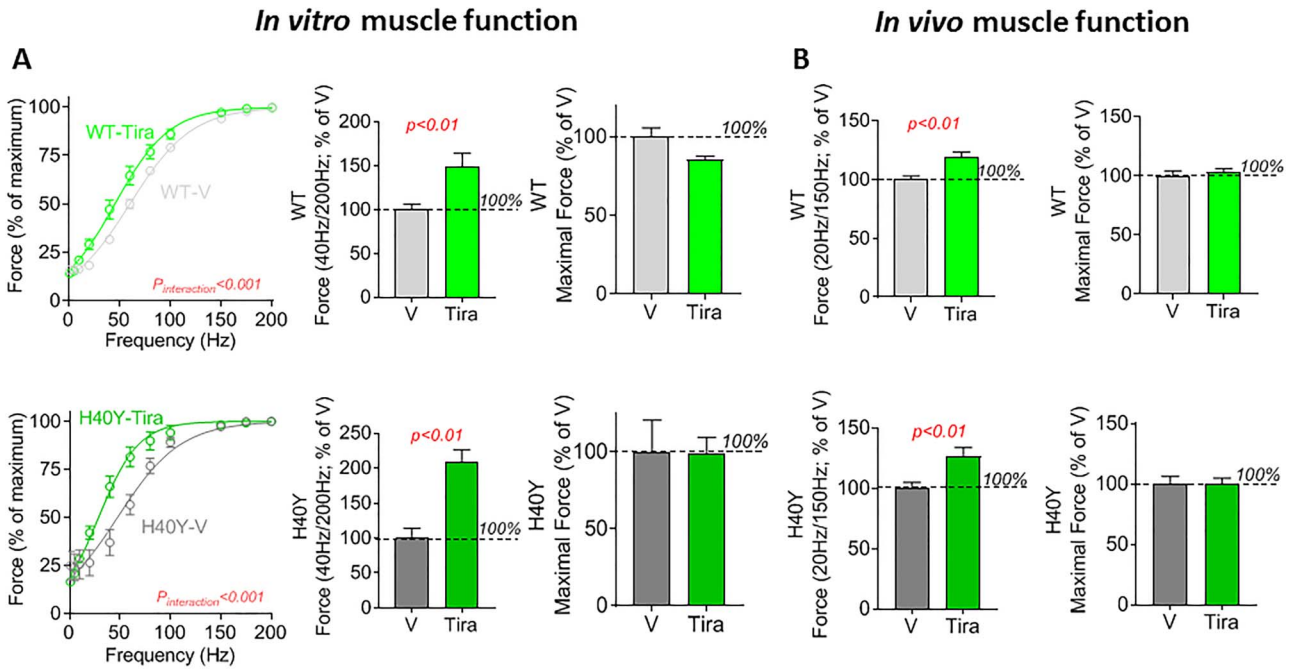


**Figure 2.** Effects of acute *tirasemtiv* (Tira) administration on *in vitro* (**A**) and *in vivo* (**B**) muscle function in *Acta1*(WT) and *Acta1*$^{H40Y}$ mice. (A) Left panels: Force-stimulation frequency relation of EDL muscle. Middle panels: The force at 40 Hz stimulation relative to that at 200 Hz stimulation. Right panels: The force at maximal stimulation (200 Hz). (B) Left panels: The force at 20 Hz stimulation relative to that at 150 Hz stimulation in *gastrocnemius* muscle. Right panels: The force at maximal stimulation (150 Hz). Note that all data are presented relative to the vehicle (V) treated group.

**Table 1.** *In vitro* muscle mechanics—acute treatment

| | Diaphragm | | EDL | |
|---|---|---|---|---|
| Frequency | 20 Hz | 150 Hz | 40 Hz | 200 Hz |
| ***Acta1*(WT)—Vehicle** | | | | |
| Absolute force (mN) | - | - | 70 ± 10 | 200 ± 20 |
| Normalized force (mN/mm$^2$) | 57 ± 8 | 143 ± 13 | 125 ± 10 | 377 ± 18 |
| Relative force (% of maximum) | 43 ± 4 | 100 ± 0.1 | 32 ± 2 | 100 ± 0 |
| ***Acta1*(WT)—*Tirasemtiv*** | | | | |
| Absolute force (mN) | - | - | 100 ± 10[a] | 180 ± 4 |
| Normalized force (mN/mm$^2$) | 76 ± 14[a] | 126 ± 14 | 160 ± 23[a] | 385 ± 27 |
| Relative force (% of maximum) | 64 ± 5[a] | 99 ± 0.4 | 47 ± 5[a] | 100 ± 0.2 |
| ***Acta1*$^{H40Y}$—Vehicle** | | | | |
| Absolute force (mN) | - | - | 4 ± 1[b] | 10 ± 10[b] |
| Normalized force (mN/mm$^2$) | 37 ± 7 | 81 ± 10[b] | 13 ± 3[b] | 34 ± 7[b] |
| Relative force (% of maximum) | 41 ± 1 | 100 ± 0.1 | 35 ± 8 | 94 ± 2[b] |
| ***Acta1*$^{H40Y}$—*Tirasemtiv*** | | | | |
| Absolute force (mN) | - | - | 20 ± 3[a] | 22 ± 5 |
| Normalized force (mN/mm$^2$) | 54 ± 11[a] | 78 ± 13 | 29 ± 5[a] | 39 ± 4 |
| Relative force (% of maximum) | 63 ± 5[a] | 100 ± 0.2 | 66 ± 6[a] | 93 ± 3 |

[a]Vehicle versus *Tirasemtiv* ($P < 0.05$)
[b]*Acta1*(WT) versus *Acta1*$^{H40Y}$ ($P < 0.05$)

mass) generated by *gastrocnemius* muscle (Fig. 4B, top panel). Absolute force values are shown in Table 4.

Subsequently, the *gastrocnemius* muscle was subjected to repetitive stimulations at 20 Hz to induce fatigue. As shown in Figure 4B (lower panel, left), in *tirasemtiv*-treated *Acta1*$^{H40Y}$ mice the force generated was higher than in vehicle-treated mice at all time points. The fatigue index was comparable between *tirasemtiv*-treated and vehicle-treated *Acta1*$^{H40Y}$ mice. Interestingly, the reduction in phosphocreatine (PCr; Fig. 4B, lower panel, right) and pH (Vehicle: from 7.08 ± 0.02 to 6.98 ± 0.01; *tirasemtiv*: from 7.13 ± 0.03 to 6.96 ± 0.05) during the fatigue protocol was comparable between *tirasemtiv*-treated and vehicle-treated *Acta1*$^{H40Y}$ mice.

Thus, chronic administration of *tirasemtiv* increased submaximal force generation. Chronic administration also increased maximal force generation, suggesting that chronic administration of *tirasemtiv* induces muscle remodeling to improve contractility. The force generated during the development of fatigue was

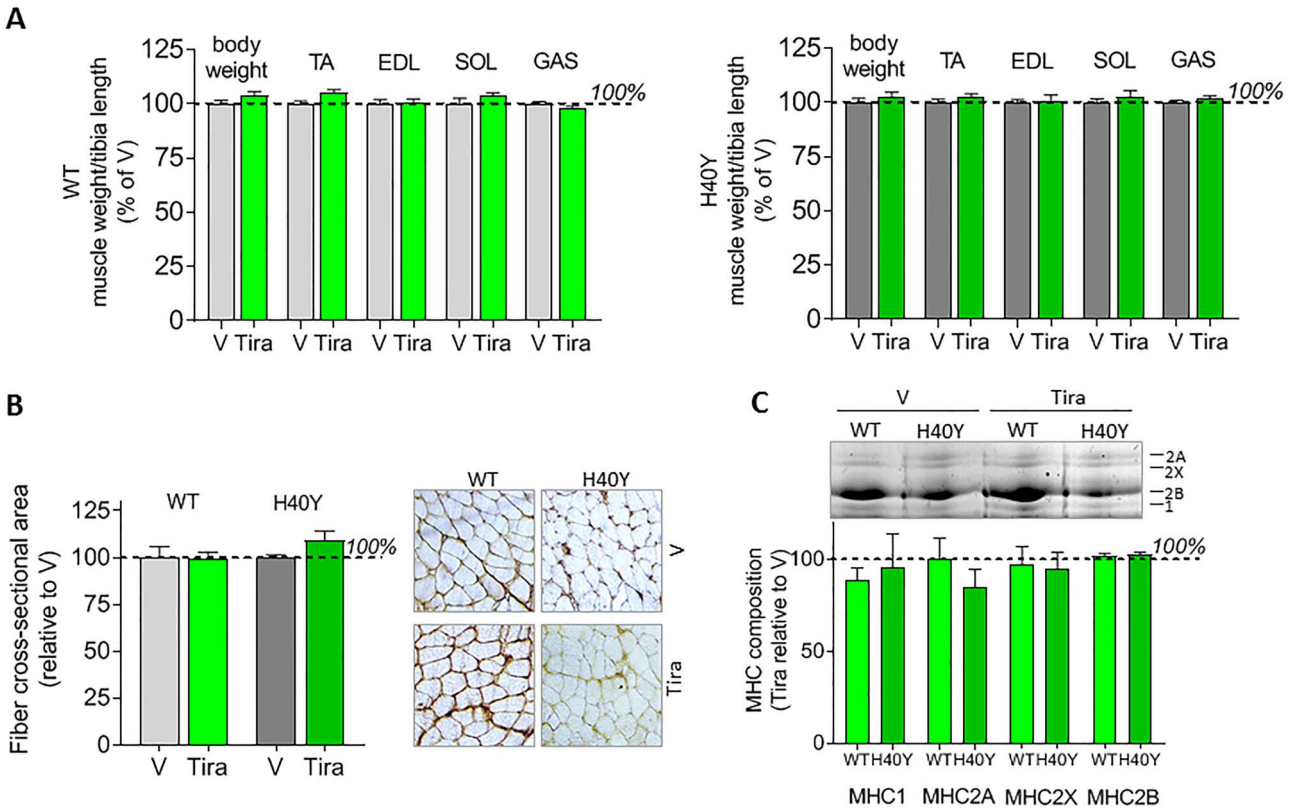


**Figure 3.** Effects of chronic *tirasemtiv* (Tira) administration on muscle mass, fiber size and fiber type distribution. (**A**) Body and wet muscle weights, normalized over tibia length, in *Acta1*(WT) (left) and *Acta1*$^{H40Y}$ (right) mice. Data are presented relative to the data from the vehicle (V) treated group. (**B**) Fiber cross-sectional area of *gastrocnemius* muscle. Right panel shows representative cryosections stained with wheat germ agglutinin to demarcate muscle fibers. Data are presented relative to the data from the vehicle (V) treated group. (**C**) The effect of chronic *tirasemtiv* administration on fiber type composition in *gastrocnemius* muscle.

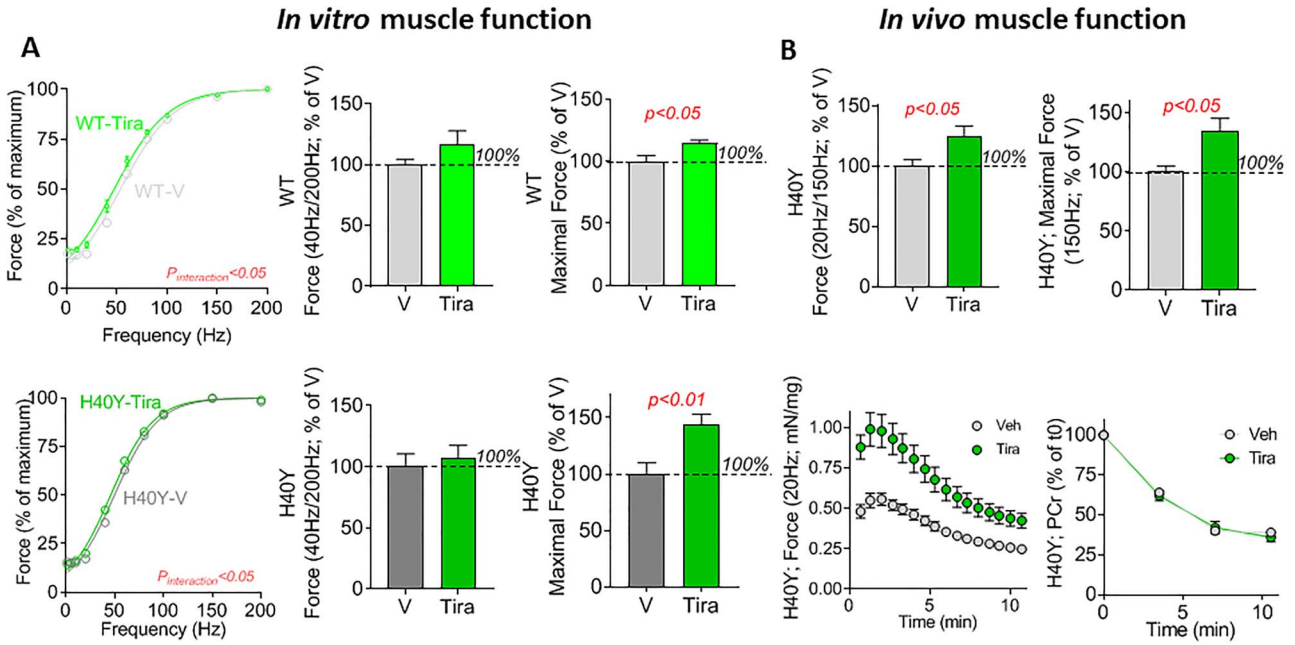


**Figure 4.** Effects of chronic *tirasemtiv* (Tira) administration on *in vitro* (**A**) and *in vivo* (**B**) muscle function. (A) Left panels: Force-stimulation frequency relation of EDL muscle. Middle panels: The force at 40 Hz stimulation relative to that at 200 Hz stimulation. Right panels: The force at maximal stimulation (200 Hz). Note that data are presented relative to the vehicle (V) treated group. (B) Top left panel: The force at 20 Hz stimulation relative to that at 150 Hz stimulation in *Acta1*$^{H40Y}$ *gastrocnemius* muscle. Top right panel: The force at maximal stimulation (150 Hz) in *Acta1*$^{H40Y}$ *gastrocnemius* muscle. Note that data are presented relative to the vehicle (V) treated group. Bottom left panel: Force of *gastrocnemius* muscle in *Acta1*$^{H40Y}$ mice during a fatigue protocol. Bottom right panel: Phosphocreatine (PCr) levels in *gastrocnemius* muscle in *Acta1*$^{H40Y}$ mice during the fatigue protocol.

**Table 2.** *In vivo* muscle mechanics—acute treatment

| Frequency | 20 Hz | 150 Hz |
|---|---|---|
| **Absolute force (mN)** | | |
| *Acta1*(WT)—Vehicle | 108 ± 3 | 367 ± 16 |
| *Acta1*(WT)—*Tirasemtiv* | 134 ± 5[a] | 377 ± 10 |
| $Acta1^{H40Y}$—Vehicle | 37 ± 3[b] | 127 ± 8[b] |
| $Acta1^{H40Y}$—*Tirasemtiv* | 47 ± 4[a,b] | 127 ± 6[b] |

[a]Vehicle versus *Tirasemtiv* ($P < 0.05$)
[b]*Acta1*(WT) versus $Acta1^{H40Y}$ ($P < 0.05$)

higher in *tirasemtiv*-treated mice, while the metabolic changes were comparable. This indicates a lower energetic cost of force generation in muscle of *tirasemtiv*-treated $Acta1^{H40Y}$ mice.

## Effect of *tirasemtiv* on the respiratory muscles

Diaphragm muscle of $Acta1^{H40Y}$ mice had a significantly larger CSA of slow-twitch fibers than *Acta1*(WT) mice (Fig. 5A). *Tirasemtiv* affects the contractility of fast-twitch muscle fibers, which express type 2 MHC isoforms. Therefore, we evaluated the MHC isoform composition of diaphragm muscles. As shown in Figure 5B, diaphragm contains ∼5% type 1 MHC, a percentage that was comparable between *Acta1*(WT) and $Acta1^{H40Y}$ mice. Thus, the vast majority of fibers expressed type 2 MHC, with type 2A MHC the most abundant one. In $Acta1^{H40Y}$ mice, there was a significant increase in fibers expressing type 2A MHC at the expense of type 2B and type 2X MHC. The maximal tetanic tension (150 Hz) generated by isolated diaphragm strips was lower in $Acta1^{H40Y}$ than in *Acta1*(WT) mice (Fig. 5C, left panel). The force-stimulation frequency curve was comparable between mice (Fig. 5C, right panel). Finally, we applied plethysmography to determine the *in vivo* functioning of the respiratory muscles. As shown in Figure 5D, tidal volume was higher in $Acta1^{H40Y}$ mice than in *Acta1*(WT) mice, and respiratory frequency was reduced in $Acta1^{H40Y}$ mice.

We evaluated the effect of acute administration of 3 μM *tirasemtiv* on the *in vitro* contractility of diaphragm strips of *Acta1*(WT) and $Acta1^{H40Y}$ mice. *Tirasemtiv* induced a leftward shift of the force-stimulation frequency curve in both *Acta1*(WT) and $Acta1^{H40Y}$ diaphragm (Fig. 6A, left panel). Consequently, the force generated at 20 Hz (normalized to maximal force at 150 Hz) was increased by 47% in *Acta1*(WT) muscle and by ∼55% in $Acta1^{H40Y}$ mice (Fig. 6A, right panel). *Tirasemtiv* did not significantly affect the maximal force generated by diaphragm muscle (Fig. 6B). Note that absolute force values are shown in Table 1.

We evaluated the effect of acute administration of 3 mg/kg *tirasemtiv* on *in vivo* function of the respiratory muscles using plethysmography. During exposure to 5% $CO_2$, *tirasemtiv* increased the tidal volume by ∼11% in both *Acta1*(WT) and $Acta1^{H40Y}$ mice compared to vehicle-treated mice (Fig. 6C). During exposure to 5% $CO_2$, *tirasemtiv* decreased respiratory frequency by ∼5% in both *Acta1*(WT) and $Acta1^{H40Y}$ mice compared to vehicle-treated mice (Fig. 6D). The data collected at room air (normal $CO_2$) as well as the absolute data are shown in Table 5.

We evaluated the effect of chronic administration of *tirasemtiv* on the *in vitro* contractility of diaphragm muscle strips of *Acta1*(WT) and $Acta1^{H40Y}$ mice. Note that after excision of the diaphragm from the mouse and prior to the contractility assay, muscles were bathed for ∼20 min in *tirasemtiv*-free Ringer solution. Previous work indicated that this time frame is sufficient to completely remove *tirasemtiv* from diaphragm muscles. The chronic administration of *tirasemtiv* did not affect the force-stimulation frequency relation in *Acta1*(WT) mice (Fig. 6E, upper left panel), and thus the ratio of force generated at 20 Hz to that at 150 Hz was comparable (Fig. 6E, upper right panel). However, in $Acta1^{H40Y}$ mice, chronic *tirasemtiv* administration induced a leftward shift of the force-stimulation curve (Fig. 6E, lower left panel), resulting in a higher force generated at 20 Hz (normalized to maximal force at 150 Hz; Fig. 6E, lower right panel). Chronic administration of *tirasemtiv* did not affect the maximal force generated by the diaphragm in *Acta1*(WT) and $Acta1^{H40Y}$ mice (Fig. 6F). Absolute force values are shown in Table 3.

We also assessed the effect of chronic *tirasemtiv* administration on *in vivo* respiratory muscle function using plethysmography. Note that during these assays, *tirasemtiv* was present in the respiratory muscles. Chronic administration of *tirasemtiv* did not affect tidal volume and respiratory frequency during exposure to 5% $CO_2$ in both *Acta1*(WT) and $Acta1^{H40Y}$ mice (Fig. 6G and H; Table 6). The data collected at room air (normal $CO_2$), as well as the absolute data, are shown in Table 6.

## Effect of chronic *tirasemtiv* administration on protein expression in gastrocnemius

We determined, in *gastrocnemius* muscle, the effect of chronic *tirasemtiv* administration on the expression of several markers of intracellular pathways involved in the regulation of muscle atrophy/hypertrophy, oxidative stress and mitochondrial structure and function (see Supplementary Material, Figs S1 and S2). Chronic administration of *tirasemtiv* increased MuRF-1 levels, but only in the $Acta1^{H40Y}$ muscles. Chronic administration of *tirasemtiv* also increased MFN1 and MFN2 levels in $Acta1^{H40Y}$ muscles, but decreased MFN1 levels in *Acta1*(WT) muscles. *Tirasemtiv* decreased OPA1 levels in *Acta1*(WT) muscles, but not in $Acta1^{H40Y}$ muscles.

## Effect of *tirasemtiv* on permeabilized quadriceps fibers of a patient with the $ACTA1^{H40Y}$ mutation

Finally, we studied the ability of *tirasemtiv* to restore the force generated at submaximal calcium levels in muscle fibers isolated from muscle of a patient harboring the $ACTA1^{H40Y}$ mutation. First, we performed histological assays in the muscle biopsy and observed in NADH-stained cryosections a relatively high proportion of fast-twitch fibers (Fig. 7A). Electron microscopy showed muscle fibers with severely damaged myofibrillar structure, nemaline rods (a hallmark feature of NEM) and nuclear rods, but also fibers with normal structure (Fig. 7B). Small bundles were permeabilized, exposed to solutions with incremental $Ca^{2+}$ concentration, and the force generated was determined. The myosin heavy chain (MHC) composition of these small bundles consists of 33% type 1 and 67% type 2 fibers. Experiments were performed in the presence and absence of 10 μM *tirasemtiv*. As shown in Figure 7C, *tirasemtiv* induced a profound leftward shift of the force-pCa relation in fast-twitch fibers, indicating increased $Ca^{2+}$ sensitivity of force. This shift was illustrated by an increase in the $pCa_{50}$ (Fig. 7C, inset). Importantly, al low, yet physiological $Ca^{2+}$ concentrations, *tirasemtiv* increased active tension in $ACTA1^{H40Y}$ fibers to values that were close to, or even exceeded those generated in fibers of healthy subjects (Fig. 7D). These findings show the promise of *tirasemtiv*

**Table 3.** *In vitro* muscle mechanics—chronic treatment

| | Diaphragm | | EDL | |
|---|---|---|---|---|
| Frequency | 20 Hz | 150 Hz | 40 Hz | 200 Hz |
| ***Acta1*(WT)—Vehicle** | | | | |
| Absolute force (mN) | - | - | 90 ± 10 | 270 ± 10 |
| Normalized force (mN/mm$^2$) | 116 ± 13 | 212 ± 11 | 136 ± 9 | 409 ± 20 |
| Relative force (% of maximum) | 53 ± 4 | 100 ± 0.4 | 33 ± 1 | 100 ± 0 |
| ***Acta1*(WT)—*Tirasemtiv*** | | | | |
| Absolute force (mN) | - | - | 130 ± 10[a] | 310 ± 10[a] |
| Normalized force (mN/mm$^2$) | 113 ± 11 | 216 ± 15 | 199 ± 14[a] | 482 ± 10[a] |
| Relative force (% of maximum) | 54 ± 2 | 100 ± 0.1 | 41 ± 3[a] | 100 ± 0 |
| ***Acta1*$^{H40Y}$—Vehicle** | | | | |
| Absolute force (mN) | - | - | 30 ± 4[b] | 80 ± 10[b] |
| Normalized force (mN/mm$^2$) | 63 ± 12[b] | 119 ± 16 | 60 ± 8[b] | 164 ± 18[b] |
| Relative force (% of maximum) | 50 ± 3 | 100 ± 0.2 | 36 ± 2 | 98 ± 1 |
| ***Acta1*$^{H40Y}$—*Tirasemtiv*** | | | | |
| Absolute force (mN) | - | - | 50 ± 5[a] | 110 ± 10[a] |
| Normalized force (mN/mm$^2$) | 78 ± 13 | 126 ± 18 | 91 ± 9[a] | 211 ± 13 |
| Relative force (% of maximum) | 60 ± 3[a] | 99 ± 0.3 | 42 ± 2[a] | 99 ± 0.3 |

[a]Vehicle versus *Tirasemtiv* ($P < 0.05$)
[b]*Acta1*(WT) versus *Acta1*$^{H40Y}$ ($P < 0.05$)

**Table 4.** *In vivo* muscle mechanics—chronic treatment

| | Week 0 | | Week 4 | |
|---|---|---|---|---|
| Frequency | 20 Hz | 150 Hz | 20 Hz | 150 Hz |
| ***Acta1*$^{H40Y}$—Vehicle** | | | | |
| Absolute force (mN) | 39 ± 3 | 179 ± 13 | 34 ± 3 | 149 ± 8[c] |
| Normalized force (mN/mg) | — | — | 0.5 ± 0.04 | 2 ± 0.1 |
| ***Acta1*$^{H40Y}$—*Tirasemtiv*** | | | | |
| Absolute force (mN) | 40 ± 5 | 177 ± 9 | 46 ± 4[a] | 165 ± 6[c] |
| Normalized force (mN/mg) | — | — | 0.8 ± 0.1[a] | 3 ± 0.2[a] |

[a]Vehicle versus *Tirasemtiv* ($P < 0.05$)
[c]Week 0 versus Week 4 ($P < 0.05$)

**Table 5.** Plethysmography—acute treatment

| | Vehicle | | *Tirasemtiv* | |
|---|---|---|---|---|
| | Rest | 5% $CO_2$ | Rest | 5% $CO_2$ |
| ***Acta1*(WT)** | | | | |
| Breathing frequency (per min) | 150 ± 5 | 214 ± 5 | 156 ± 3 | 211 ± 2 |
| Tidal volume (ml/kg) | 10 ± 0.2 | 14 ± 0.3 | 10 ± 0.3 | 15 ± 0.3[a] |
| Minute volume (ml/kg/min) | 1444 ± 49 | 2921 ± 114 | 1551 ± 48 | 3191 ± 60 |
| ***Acta1*$^{H40Y}$** | | | | |
| Breathing frequency (per min) | 145 ± 4 | 209 ± 3 | 144 ± 2[b] | 203 ± 5 |
| Tidal volume (ml/kg) | 12 ± 0.3[b] | 17 ± 0.5[b] | 12 ± 0.2[b] | 18 ± 0.4[a,b] |
| Minute volume (ml/kg/min) | 1666 ± 61[b] | 3466 ± 118[b] | 1708 ± 50 | 3735 ± 116[b] |

[a]Vehicle versus *Tirasemtiv* ($P < 0.05$)
[b]*Acta1*(WT) versus *Acta1*$^{H40Y}$ ($P < 0.05$)

in restoring muscle strength in patients with the *ACTA1*$^{H40Y}$ mutation.

## Discussion

In skeletal muscles of mice with the *Acta1*$^{H40Y}$ mutation, acute *in vitro* or *in vivo* treatment with *tirasemtiv* increased the force response to submaximal stimulation frequencies. The increase in muscle force at submaximal stimulation persisted following chronic treatment of *Acta1*$^{H40Y}$ mice with *tirasemtiv*. Furthermore, $^{31}$P-MRS revealed that the increased force generation during treatment with *tirasemtiv* did not increase muscle energy consumption, indicating that the energetic cost of force generation was reduced in muscle of *tirasemtiv*-treated *Acta1*$^{H40Y}$ mice. Chronic treatment of *Acta1*$^{H40Y}$ mice with *tirasemtiv* also increased the force response to *maximal* stimulation, with no muscle mass increase. This suggests that muscle remodeling had occurred to improve contractility. Finally, studies on muscle

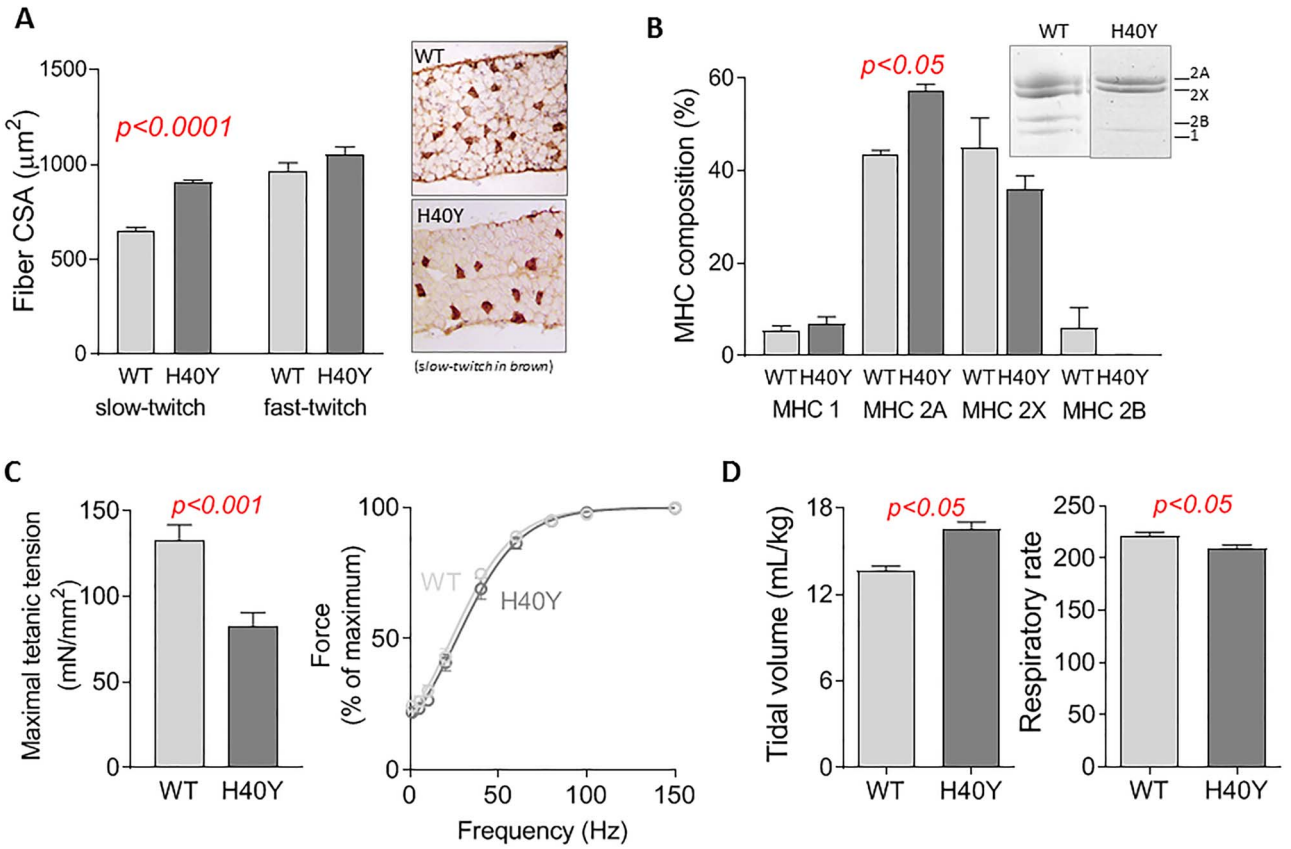


**Figure 5.** Characterization of respiratory muscles in the *Acta1*$^{H40Y}$ mouse model. (**A**) Diaphragm fiber cross sectional area; left panel shows typical diaphragm cryosections stained to identify slow-twitch muscle fibers. (**B**) MHC isoform composition in the diaphragm muscle as determined by SDS-PAGE. Inset: a typical SDS-PAGE result showing separation of the four isoforms. (**C**) Left panel: *In vitro* maximal tension of diaphragm strips stimulated with 150 Hz. Right panel: the force-stimulation frequency relation of diaphragm strips. (**D**) *In vivo* respiratory function, as determined by whole body plethysmography. Left panel shows tidal volume and right panel shows respiratory rate.

**Table 6.** Plethysmography—chronic treatment

| | Week 0 | | Week 4 | |
|---|---|---|---|---|
| | Rest | 5% $CO_2$ | Rest | 5% $CO_2$ |
| ***Acta1*(WT)—Vehicle** | | | | |
| Breathing frequency (per min) | 174 ± 3 | 249 ± 3 | 166 ± 4 | 249 ± 2 |
| Tidal volume (ml/kg) | 11 ± 0.2 | 16 ± 0.3 | 10 ± 0.2[c] | 16 ± 0.2 |
| Minute volume (ml/kg/min) | 1846 ± 50 | 4090 ± 108 | 1618 ± 42[c] | 3934 ± 67 |
| ***Acta1*(WT)—*Tirasemtiv*** | | | | |
| Breathing frequency (per min) | 168 ± 4 | 261 ± 4[a] | 159 ± 3 | 244 ± 3[c] |
| Tidal volume (ml/kg) | 11 ± 0.3 | 17 ± 0.3 | 10 ± 0.2 | 16 ± 0.2 |
| Minute volume (ml/kg/min) | 1797 ± 71 | 4282 ± 108 | 1656 ± 57 | 4014 ± 98[c] |
| ***Acta1*$^{H40Y}$—Vehicle** | | | | |
| Breathing frequency (per min) | 157 ± 5[b] | 247 ± 5 | 144 ± 3[b,c] | 237 ± 5[b] |
| Tidal volume (ml/kg) | 13 ± 0.3[b] | 20 ± 0.5[b] | 12 ± 0.4[b] | 19 ± 0.6[b] |
| Minute volume (ml/kg/min) | 2015 ± 76 | 4894 ± 198[b] | 1767 ± 71[c] | 4551 ± 189[b] |
| ***Acta1*$^{H40Y}$—*Tirasemtiv*** | | | | |
| Breathing frequency (per min) | 157 ± 5 | 245 ± 5 | 141 ± 4[c] | 234 ± 4[c] |
| Tidal volume (ml/kg) | 12 ± 0.3 | 19 ± 0.3 | 12 ± 0.4 | 20 ± 0.4[a,c] |
| Minute volume (ml/kg/min) | 1879 ± 86 | 4530 ± 171 | 1677 ± 59 | 4527 ± 117 |

[a]Vehicle versus *Tirasemtiv* ($P < 0.05$)
[b]*Acta1*(WT) versus *Acta1*$^{H40Y}$ ($P < 0.05$)
[c]Week 0 versus Week 4 ($P < 0.05$)

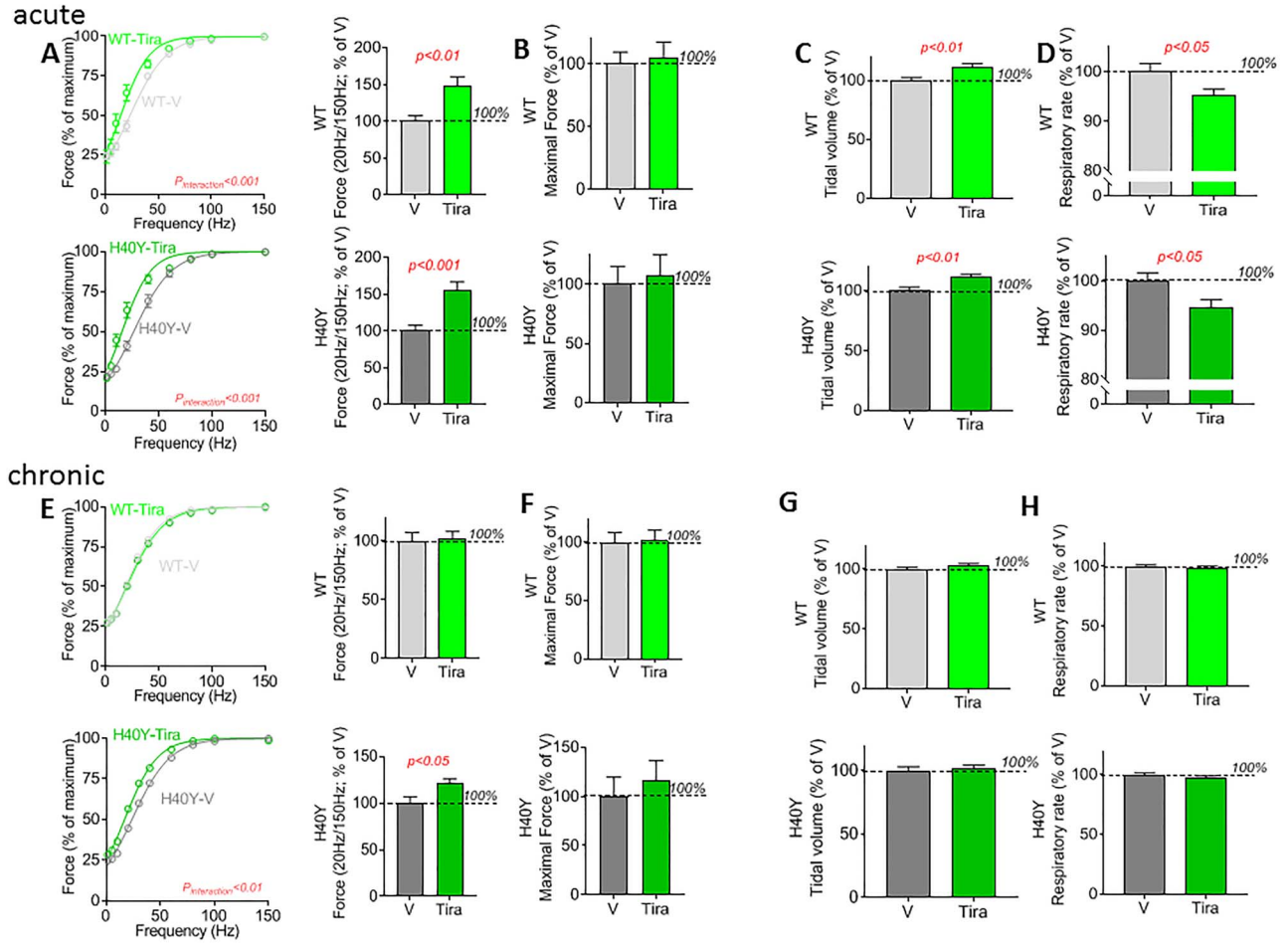


**Figure 6.** Effect of acute and chronic *tirasemtiv* administration on respiratory muscle function in *Acta1*(WT) and *Acta1*$^{H40Y}$ mice. (**A** and **E**) Left panels: Force-frequency stimulation relations during acute and chronic treatment with *tirasemtiv*. Right panels: The force at 20 Hz stimulation relative to that at 150 Hz stimulation. (**B** and **F**) The force at maximal stimulation (150 Hz). (**C** and **G**) Tidal volume as determined by whole body plethysmography. (**D** and **H**) Respiratory rate as determined by whole body plethysmography. Note that data is presented relative to the vehicle (V) treated group.

fibers from a patient with the *ACTA1*$^{H40Y}$ mutation revealed that, at physiological $Ca^{2+}$ concentrations, *tirasemtiv* increased force generation to values that were close to those generated in muscle fibers of healthy subjects. Together, these findings indicate the therapeutic potential of fast skeletal troponin activators to alleviate muscle weakness in patients with the *ACTA1*$^{H40Y}$ mutation.

## The effect of *tirasemtiv* persists during chronic treatment of *Acta1*$^{H40Y}$ mice

NEM is a congenital myopathy, which, in the majority of cases, is caused by mutations in genes encoding proteins of the skeletal muscle thin filament (16). The most severely affected patients fail to survive beyond the first year of life due to severe muscle weakness. The mechanisms underlying muscle weakness have gained widespread attention during the past years. These include disturbed interactions between the thin and thick filaments, reduced length of the thin filaments, muscle fiber hypotrophy and myofibrillar disarray (17–19,27–29). To date, no specific therapies are available for NEM patients. Considering the central role of the thin filament in the NEM pathology, targeting the functioning of this sarcomeric microstructure might prove an effective approach (1). Therefore, we tested the ability of *tirasemtiv*, a fast skeletal muscle troponin activator that specifically targets the troponin complex on the thin filament (24), to alleviate muscle weakness in NEM. We hypothesized that fast skeletal troponin activation would augment the force response to *submaximal* stimulation frequencies. These are clinically relevant frequencies considering that during daily life activities the force levels of muscle range between 10% and 65% of its maximal level (30). To test this hypothesis, we made use of the *Acta1*$^{H40Y}$ mouse model, a knock-in mouse with a mutation (p.His42Tyr) in the $\alpha$-skeletal actin gene that causes a dominantly inherited severe form of the disease in humans (25). In line with our hypothesis, we found that acute administration of *tirasemtiv* markedly increases force generation at submaximal stimulation frequencies, with a more than 25% increase of force in *gastrocnemius* muscle *in vivo* (Fig. 2B). This effect is comparable to that found in previous work in a nebulin-based NEM mouse model (26). The magnitude of the increase was comparable to that observed after 4 weeks of chronic *tirasemtiv* treatment via chow (Fig. 4B), which is an important finding as it indicates that long-term administration of *tirasemtiv* does not desensitize the muscles to its effect. In addition to the persistent positive inotropic effect of chronic *tirasemtiv* treatment at submaximal stimulation frequencies, both EDL and *gastrocnemius* muscles showed increased force at maximal

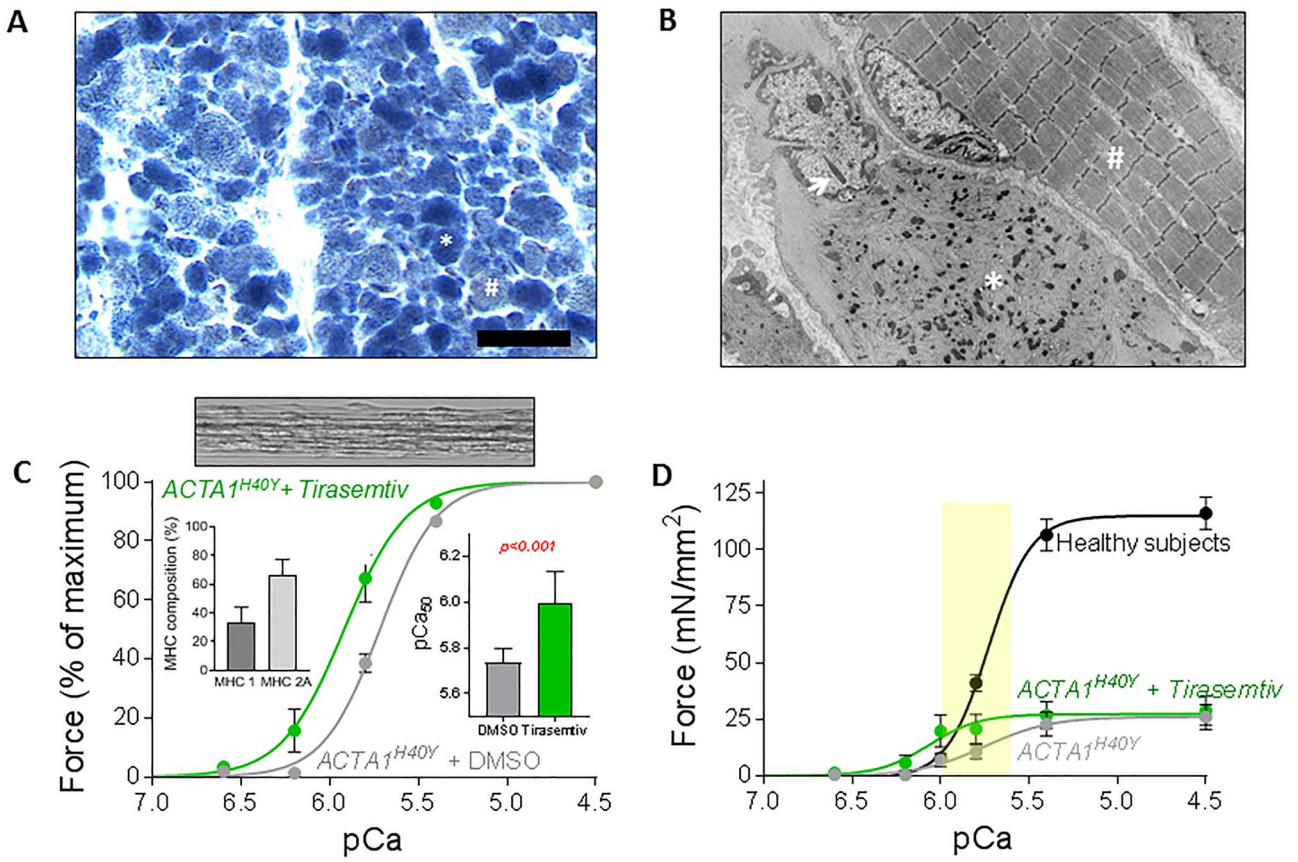


**Figure 7.** Effect of *tirasemtiv* on the contractility of permeabilized quadriceps fibers of a patient with *ACTA1*$^{H40Y}$ mutation. (**A**) NADH stained cryosection of the patient's muscle biopsy. The cryosection shows both slow-twitch (dark; *) and fast-twitch (light; #) muscle fibers. Bar: 100 µm. (**B**) electron microscopy image showing a fiber with severely damaged myofibrillar structure, nemaline rods (*) and a nuclear rod (arrow), and a fiber with preserved ultrastructure (#). (**C**) The relative force-pCa relation of permeabilized muscle fibers isolated from the patient's biopsy (inset at top shows a typical bundle of 5–10 fibers used for the contractility assays; left bar graph shows the MHC composition of the muscle bundles; rightbar graph shows the *tirasemtiv*-induced shift in the $pCa_{50}$, i.e. the pCa required to generate 50% of maximal force). (**D**) The tension-pCa relation of treated and untreated permeabilized muscle fibers from the patient, compared to the tension-pCa relation of muscle fibers from healthy subjects. The yellow bar indicates the physiological calcium concentration in muscle fibers during normal contractility.

stimulation frequencies (increase in EDL: ~43%, in *gastrocnemius*: ~35%; Fig. 4). This finding is not explained by the direct effects of *tirasemtiv*, as at saturating calcium concentrations *tirasemtiv* does not augment force generation (24). Indeed, this inotropic effect was not observed during acute treatment with *tirasemtiv* (Fig. 2). Thus, this finding indicates that, during chronic *tirasemtiv* treatment, the EDL and *gastrocnemius* muscles adapt by structural remodeling.

The nature of this remodeling is not clear (it does not include increased muscle fiber size or muscle mass, or changes in fiber type proportion; Fig. 3). It is tempting to speculate that the positive inotropic effects of *tirasemtiv* improved the myofibrillar structure in muscle fibers. Damaged myofibrillar proteins are labeled by chains of ubiquitin molecules, which mark them for degradation by the proteasome (31). Several major myofibrillar proteins, including myosin, are ubiquitinated by MuRF1 (32). We observed that in the *Acta1*$^{H40Y}$ mice, chronic *tirasemtiv* treatment increased the levels of MuRF1 (Supplementary Material, Fig. S2). This increase in MuRF1 protein might have facilitated the degradation of damaged proteins in *Acta1*$^{H40Y}$ mice, thereby improving the myofibrillar ultrastructure and force generation. Another mechanism via which *tirasemtiv* might have increased the force generating capacity of muscle following chronic treatment could be based on post-translational modifications of myofibrillar proteins, such as oxidation and nitrosylation. Both of them have been shown to be able to affect force production (33,34). Our results rule out the possibility that a *tirasemtiv*-induced decrease in the oxidation of myosin or other proteins is involved (Supplementary Material, Fig. S1), but leave open the possibility that other post-translational modifications play a role.

### *Tirasemtiv* reduces the energetic cost of contraction in *Acta1*$^{H40Y}$ mice

The benefit from fast skeletal troponin activators, such as *tirasemtiv*, involves both increased force development and lower energy cost of contraction. In the present study, we showed, using *in vivo* $^{31}$P-MRS in *Acta1*$^{H40Y}$ mice, that chronic treatment with *tirasemtiv* increased force generation of *gastrocnemius* muscles during a fatigue protocol at a stimulation frequency of 20 Hz. Such an increase is very likely due to *tirasemtiv* reducing the off-rate of $Ca^{2+}$ from fast skeletal muscle troponin, with no effect on $Ca^{2+}$ release and cytosolic $Ca^{2+}$ concentrations (35). Importantly, the *tirasemtiv*-induced increase in force was not accompanied by a faster decay in muscle PCr concentration, suggesting a similar energy consumption rate in treated and untreated muscles (Fig. 4B). As we assume that cytosolic $Ca^{2+}$ content did not vary (35)—note that force was measured at set stimulation frequencies—the energy required by SERCA to

re-uptake $Ca^{2+}$ should be comparable in treated and untreated muscles. Energy utilization of SERCA pumps accounts for a relevant portion, 30–40%, of total ATP consumption during contraction (36). Therefore, similar SERCA ATP utilization in the presence of higher force could play a significant role in the similar PCr depletion between treated and untreated muscles, and therefore in the lower energy cost of contraction in treated muscles. In line with our reasoning, it has been previously shown that CK-2066260, a fast skeletal muscle troponin activator similar to *tirasemtiv*, decreases ATP utilization and glycogen consumption in contractions developing the same force, rendering the muscle more efficient and fatigue-resistant (35).

Another mechanism via which *tirasemtiv* might have enabled more force production with similar PCR consumption is by enhancing mitochondrial fusion (upregulation of MFN1 and MFN2, Supplementary Material, Fig. S2), which in turn could improve mitochondrial function and ATP production. Whether this mechanism plays a role requires further studies.

Thus, *tirasemtiv* ameliorates the energy cost of contraction in muscles from *Acta1*$^{H40Y}$ mice, possibly through optimization of ATP consumption of SERCA pumps and/or through the production of more ATP by mitochondria. This effect is very important for daily-life activities of NEM patients, considering that muscle fatigue is one of their major complaints.

### *Tirasemtiv* improves diaphragm contractility

NEM patients have reduced spirometric values, and consequently some patients may suffer from the sensation of dyspnea (37–39) and die from respiratory failure. Thus, weakness of the respiratory muscles is prominent in NEM (note that the contractility of the diaphragm was significantly impaired in *Acta1*$^{H40Y}$ mice; Fig. 5C) and augmenting respiratory muscle contractility can be of great benefit to patients. Therefore, in our work we also studied the effect of *tirasemtiv* on the respiratory muscles. Acute treatment with *tirasemtiv* improved the force response of the diaphragm to submaximal stimulation frequencies (Fig. 6B). Furthermore, using unrestrained whole body plethysmography, we found that *tirasemtiv* increased tidal volume (and decreased respiratory frequency to maintain minute volume; Fig. 6C and D). These effects on tidal volume are in line with previous work on a mouse model for amyotrophic lateral sclerosis (40). However, unlike the persisting effect of *tirasemtiv* on leg muscle contractility from chronic treatment (Fig. 4), the positive inotropic effect on respiratory muscle function did not persist following chronic treatment (except for a 20% increase in the force response to submaximal stimulation; Fig. 6E). We speculate that since tidal volume was not reduced in *Acta1*$^{H40Y}$ mice—even slightly increased (Fig. 5)—there was no physiological need to modulate tidal volume. Thus, as tidal volume was maintained, the energy cost of contraction of the respiratory muscles must have been reduced in the *tirasemtiv*-treated mice, an important benefit which in patients could attenuate the development of respiratory failure. Unfortunately, we could not assess energy consumption in the diaphragm using $^{31}$P-MRS. We cannot explain why *tirasemtiv* increased tidal volume during acute treatment (Fig. 6C). We speculate that this increase was transient, and that the monitoring time (30 min) might not have been sufficiently long for the mice to adapt their respiratory mechanics to the positive inotropic effects of *tirasemtiv* on the inspiratory muscles.

### Clinical perspective

The positive inotropic effect of *tirasemtiv* in the *Acta1*$^{H40Y}$ mouse model was mimicked in a patient biopsy with the *ACTA1*(H40Y) mutation. At physiological calcium concentrations, the force generated by the patient's fibers nearly doubled in the presence of *tirasemtiv* (Fig. 7), and reached values that were close to those of healthy subjects. Although, recently, *tirasemtiv* did not meet its primary endpoint in a phase 3 clinical trial in ALS patients in part due to its side effect profile, including dizziness (41), our findings illustrate the great therapeutic promise of fast skeletal muscle troponin activation. *Reldesemtiv,* a newer fast skeletal muscle troponin activator, does not appear to exhibit the same side effect profile as *tirasemtiv* and is currently being developed and tested for efficacy in clinical trials (35,42–45). Fast skeletal muscle troponin activators target fast-twitch muscle fibers. The improved contractility of these fibers improves strenuous muscle exercise as well as coughing and airway clearance—both major challenges for NEM patients—as these maneuvers are accomplished through the recruitment of fast-twitch fibers. It is possible that in patients, the magnitude of the effect of *tirasemtiv* is blunted by slow-twitch fiber predominance, a common feature of NEM (1). The patient's fiber bundles studied here consisted of a mix of slow- and fast-twitch fibers, with predominance of fast-twitch fibers. Consequently, the effect of *tirasemtiv* was large (Fig. 7). Clearly, the effect size will decrease with slow-twitch fiber predominance. However, although NEM patients display a heterogeneous phenotype, fatigue and dyspnea are common complaints. Thus, even a modest improvement of diaphragm muscle function would benefit NEM patients and attenuate the development of dyspnea and respiratory failure, the major cause of death in NEM. Clearly, NEM patients might also benefit from the recruitment of slow-twitch fibers. During normal breathing and low intensity exercises, these fibers are first recruited. An additional advantage of recruiting slow-twitch fibers is the above-mentioned slow-twitch fiber predominance in NEM patients. Levosimendan is a calcium sensitizer that is approved for human use by the European Medicines Agency for acutely decompensated severe chronic heart failure. It exerts its effect through binding to slow skeletal/cardiac troponin C, which is also the dominant troponin C isoform in slow-twitch skeletal muscle fibers. However, previous studies showed no inotropic effect of levosimendan on slow-twitch fibers of NEM patients (46). Furthermore, a disadvantage of compounds that target slow skeletal/cardiac troponin C might be that they also affect cardiac function. To date, no activators specific for TnC in slow-twitch skeletal muscle fibers—with no effect on cardiomyocytes—have been developed. Alternatively, future studies might address the development of activators that target slow skeletal TnI, which is exclusively expressed in skeletal muscle.

## Materials and Methods

### *Acta1*$^{H40Y}$ knock-in mouse model

Mice with the heterozygous NM_009606.3(Acta1):p.His42Tyr mutation in *Acta1* (referred to as *Acta1*$^{H40Y}$ to be consistent with existing literature utilizing an older numbering scheme) and wild-type (WT) littermates were used for the experiments, a well-established NEM knock-in mouse model (25,47,48). Experiments were conducted in agreement with the French and Dutch guidelines for animal care. All animal experiments were approved by the Institutional Animal Care Committee of Aix-Marseille University (#15–14 052 012) and by the local animal ethics committee at VU University (AVD114002016501).

Experiments were only performed on females given that the majority of males typically die within the first 6–8 weeks after birth (25). Mice were housed in an environment-controlled facility (12–12 h light–dark cycle, 22°C), received water and standard food *ad libitum*. Mice were identified through PCR genotyping from mouse tail DNA.

### *Tirasemtiv* treatment

For the studies in which the acute effects of *tirasemtiv* were studied, mice were I.P. injected with vehicle or 3 mg/kg *tirasemtiv* (40). Experiments were performed ∼30 min after injection. For the experiments in which muscle contractility was studied *in vitro*, 10 μM *tirasemtiv* was added to the experimental solutions.

For the studies in which the chronic effects of *tirasemtiv* were studied, mice were first fed for 1 week with custom-made mouse pellets (BioServ). After 1 week, mice were switched to the same pellets containing *tirasemtiv* (600 ppm), or the same pellets without *tirasemtiv*. Mice were kept on the chow for 4 weeks. Mice were tested before treatment and after 4 weeks of *tirasemtiv*-enriched diet or regular diet. After 4 weeks, mice were euthanized and tissues were collected, i.e. *tibialis anterior* (TA), *extensor digitorum longus* (EDL), *soleus* (SOL), *gastrocnemius* and diaphragm (DIA).

### *In vitro* characterization of intact muscle

*In vitro* characterization of intact muscle was performed as described previously (20,49). The experimental protocols consisted of a full tetanus at 150 Hz and a force-frequency protocol.

For the force-frequency protocol, the muscle was stimulated with incremental stimulation frequencies (diaphragm: 1, 5, 10, 20, 30, 40, 60, 80, 100, 150 Hz; EDL: 1, 5, 10, 20, 40, 60, 80, 100, 150, 200 Hz). Data were discarded when stimulation at 150 Hz rendered a force that was less than 95% of the force generated during the first stimulation at 150 Hz. Stimuli were applied with a train duration of 600 ms. The resting interval was 30 s between the stimulations at 1 and 10 Hz; 60 s after stimulation at 20 Hz; 90 s after stimulation at 30 Hz; and 120 s between stimulations at 50, 70, 100 and 150 Hz.

After completion of the contractility measurements, the length and weight of the muscles were determined. CSA (in $mm^2$) was calculated by dividing muscle weight (g) by muscle length (mm) multiplied by specific density (1.056 g/ml) × 100.

### Plethysmography

Mice were placed in unrestrained whole body plethysmography chambers for 30 min of acclimation. After acclimation, tidal volume, respiratory frequency and minute ventilation were monitored for 15 min at room air. After 15 min, mice were exposed to a 5% $CO_2$ gas mixture for 30 min and monitored. After the 5% $CO_2$ exposure, mice were re-exposed to room air for 15 min and monitored (40).

### *In vivo* investigations of the plantar flexor muscles

Animal preparation: Mice were anaesthetized and individually placed supine in a home-built cradle specially designed for the strictly non-invasive functional investigation of the left hindlimb muscles as described previously (50).

Force output measurements: Non-invasive transcutaneous electrical stimulation was first elicited with square-wave pulses (0.5 ms duration) on the plantar flexor muscles. The individual maximal stimulation intensity was determined by progressively increasing the stimulus intensity until there was no further peak twitch force increase. Plantar flexion force was assessed in response to incremental frequencies (1–150 Hz; train duration = 0.75–1 s) and during a fatigue protocol (80 contractions; 20 Hz; 1.5 s on, 6 s off).

The peak force of each contraction was measured. Regarding the fatigue protocol, the corresponding tetanic force was averaged every five contractions. A fatigue index corresponding to the ratio between the last five and the first five contractions was determined. For chronic experiments, the resulting force was divided by the soleus and gastrocnemius muscle weight in order to obtain specific force (in mN/mg).

Experiments were performed in a 4.7-Tesla (T) horizontal superconducting magnet (47/30 Biospec Avance, Bruker, Ettingen, Germany) equipped with a Bruker 120 mm BGA12SL (200 mT/m) gradient insert.

Metabolic changes were investigated using $^{31}$Phosphorus-MR Spectroscopy ($^{31}$P-MRS) at rest and during the fatiguing protocol. Spectra from the *gastrocnemius* muscle region were continuously acquired at rest and throughout the fatigue protocol. A total of 495 free induction decays (FID) were acquired (TR = 2 s).

Data were processed using proprietary software developed using IDL (Interactive Data Language, Research System, Inc., Boulder, CO, USA). The first 180 FID were acquired at rest and summed together ($n = 1$, time resolution = 6 min). The next 315 FID were acquired during the stimulation period and summed by blocks of 105 ($n = 3$, time resolution = 3.5 min). Relative concentrations of high-energy phosphate metabolites (phosphocreatine (PCr) and inorganic phosphate (Pi)) were obtained by a time-domain fitting routine using the AMARES-MRUI Fortran code and appropriate prior knowledge of the ATP multiplets. Intracellular pH ($pH_i$) was calculated from the chemical shift of the Pi signal relative to PCr (51).

### Muscle fiber cross-sectional area analysis

Muscle fibre CSA was determined in the mid-belly region of *gastrocnemius* and EDL muscles and in a portion of diaphragm muscle (52). Briefly, muscle serial transverse sections (10 μm thick) were obtained from each muscle and were immunostained with monoclonal antibodies against MHC isoforms (BA-F8 against MHC-1 and SC-71 against MHC-2A). The cryosections were incubated with primary antibody for 1 h at 37°C, rinsed with PBS buffer and incubated in a secondary rabbit anti-mouse antibody conjugated with peroxidase (DAKO, Denmark) for 1 h at 37°C. After washing in PBS buffer, the stain was visualized by using a DAB (3,3′-Diaminobenzidine) solution. Images of the stained sections were captured from a light microscope (LeicaDMLS) equipped with a camera (Leica DFC 280). Fibre CSA was measured with Image J analysis software (NIH, Bethesda, MD, USA) and expressed in micrometers squared.

### MHC isoforms composition

Frozen muscles were pulverized in a steel mortar with liquid nitrogen to obtain a powder that was immediately resuspended in Laemmli solution (53). The samples were incubated in ice for 20 min and finally spun at 18 000*g* for 30 min. Protein concentration in the dissolved samples was determined with a protein assay kit (RC DC Biorad). About 10 μg of proteins for each sample were loaded on 8% SDS-PAGE polyacrylamide gels and the electrophoresis was run overnight at 250 V. Following

a Coomassie stain, four bands corresponding to MHC isoforms were separated and their densitometric analysis was performed to assess the relative proportion of MHC isoforms (MHC-1, MHC-2A and MHC-2X) in the samples (54).

### Western blot analysis

Frozen muscle samples were pulverized and immediately re-suspended in a lysis buffer (20 mM Tris–HCl, 1% Triton X100, 10% glycerol, 150 mM NaCl, 5 mM EDTA, 100 mM NaF and 2 mM NaPPi supplemented with 1× protease, phosphatase inhibitors (Sigma-Aldrich) and 1 mM PMSF). The homogenate obtained was kept on ice for 20 min and then centrifuged at 18 000*g* for 20 min at 4°C. The supernatant was stored at −80°C until ready to use. Protein concentration was evaluated for each sample and equal amounts of muscle samples were loaded on gradient precast gels purchased from Bio-Rad (AnyKd; Hercules, CA, USA). After the gel run, proteins were electro-transferred to PVDF membranes at 35 mA overnight. The membranes were incubated in 5% Milk for 2 h, rinsed with TBST buffer (0.02 M Tris and 0.05 M NaCl, pH 7.4–7.6) and subsequently probed with specific primary antibodies (see below). Thereafter, the membranes were incubated in HRP-conjugated secondary antibody. The protein bands were visualized by an enhanced chemiluminescence method in which luminol was excited by peroxidase in the presence of $H_2O_2$ (ECL Select, GE Healthcare). The content of each protein investigated was assessed by determining the brightness–area product of the protein band (55).

Antibodies used were: anti-rabbit GAPDH (1:2000 Abcam); anti-rabbit Catalase (1:1000 Abcam); anti-mouse SOD1 (1:1000 Abcam); anti-rabbit FIS1 (1:1000 Abcam); anti-rabbit p-DRP1$_{(ser616)}$ (1:1000 Cell Signalling); anti-rabbit p-DRP1$_{(ser637)}$ (1:1000 Cell Signalling); anti-rabbit DRP1 (1:3000 Cell Signalling); anti-mouse MFN1 (1:1000 Abcam); anti-rabbit MFN2 (1:1000 Abcam); anti-rabbit OPA1 (1:3000 Abcam); anti-mouse IgG (1:5000 Dako North America Inc., Carpinteria, CA, USA); anti-rabbit IgG (1:10 000 Cell Signaling).

### Carbonylated proteins analysis

Frozen samples from each subject group were suspended in a lysis buffer (50 mM Tris–HCl pH 7.6, 250 mM NaCl, 5 mM EDTA protease inhibitor cocktail and phosphatase inhibitor cocktail), left on ice for 20 min and finally centrifuged at 18 000*g* for 20 min at 4°C. Protein concentration was determined using the RC DC TM protein assay kit (Biorad product). The protein carbonylation level was detected using the OxyBlot TM Kit (Millipore) that provides reagents for sensitive immunodetection of carbonyl groups. Carbonyl groups in the protein side chains were derivatized to 2,4-dinitrophenylhydrazone (DNP) by reaction with 2,4-dinitrophenylhydrazine (DNPH). In detail, 10 µg of proteins for each muscle sample were denatured with SDS solution at a final concentration of 6%. The DNPH solution was added to obtain the derivation; the reaction was stopped after 10 min of incubation at room temperature. The DNP-derivatized protein samples were separated by polyacrylamide gel electrophoresis (Anykd Biorad gels) followed by western blotting. Proteins were transferred to nitrocellulose membranes at 100 V for 2 h, stained with Ponceau Red (Sigma) and then scanned. The membranes were blocked by incubation with 3% bovine serum albumin (BSA) for 1 h; then incubated with rabbit anti-DNP antibody overnight at 4°C and subsequently with a horseradish peroxidase-antibody conjugate (goat anti-rabbit IgG). The positive bands were visualized by using a chemiluminescent reagent (ECL advance as described previously (55). The total protein carbonylation level and the MHC carbonylation level were analyzed quantitatively by comparison of the signal intensity of immune-positive proteins normalized on total proteins amount loaded on gels (Ponceau staining signal) (55).

### Gene expression analysis

Total RNA was extracted from *gastrocnemius* muscles using an SV Total RNA isolation kit (Promega, Madison, WI, USA). The RNA concentration was measured using a Nano Drop instrument (ThermoScientific, Waltham, MA, USA) and 400 ng was used to generate cDNA with SuperScript III reverse transcriptase (Invitrogen, Carlsbad, CA, USA). The cDNA was analyzed by quantitative RT-PCR (Applied Biosystems AB7500) using a SYBR Green PCR kit (Applied Biosystems, Foster City, CA, USA) and the data were normalized to GAPDH content. Oligonucleotide primers were provided by Sigma Aldrich and were: MuRF-1 (FP: ACCTGCTGGTGGAAAACATC, RP: ACCTGCTGGTGGAAAACATC) and Atrogin-1 (FP: GCAAACACTGCCACATTCTCTC, RP: CTTGAGGGGAAAGTGAGACG). Differentially expressed genes were determined using a default threshold of 0.6. The difference between Ct (cycle threshold) values was calculated for each mRNA by taking the mean Ct of duplicate reactions and subtracting the mean Ct of duplicate reactions for the reference RNA measured on an aliquot from the same RT reaction (ΔCt = Cttarget gene—Ct reference gene). All samples were then normalized to the ΔCt value of a calibrator sample to obtain a ΔΔCt value (ΔCt target—ΔCt calibrator) (comparative method) (55).

### Patient muscle biopsies

Quadriceps muscle specimens, remaining from diagnostic procedures, was collected from a patient with the NM_001100.3 (ACTA1)His42Tyr mutation in *ACTA1* (*ACTA1*$^{H40Y}$, case 86-1 from Agrawal and coworkers (56)). Ethical approval was obtained from the Human Research Ethics Committees of the Boston Children's Hospital Institutional Review Board. Quadriceps biopsies from six adult control subjects with no medical history were obtained. All biopsies were collected following informed consent supervised by the Radboud University Institutional Review Board (20). All biopsies were stored frozen and unfixed at −80°C until use.

### Permeabilized muscle fiber mechanics in patient biopsy

Small strips were dissected from the muscle biopsies, permeabilized overnight and mechanical experiments were performed as described previously (18–20). As the contractile properties of muscle fibers are influenced by the MHC composition of the muscle fibers, we used a specialized SDS-PAGE technique to analyze the MHC isoform composition in the muscle fibers used in contractility experiments (57). In brief, muscles fibers were denatured by boiling for 2 min in SDS sample buffer. The stacking gel contained a 4% acrylamide concentration (pH 6.7), and the separating gel contained 7% acrylamide (pH 8.7) with 30% glycerol (v/v). The gels were run for 24 h at 15°C and a constant voltage of 275 volt. Finally, the gels were silver-stained, scanned, and analyzed with ImageQuant TL (GE Healthcare, Chicago, IL) software.

To test the effect of *tirasemtiv* on the calcium sensitivity of force, patient fibers were exposed to solutions with varying pCa's (protocol as described above) and in the presence/absence of *tirasemtiv* (10 µM; concentration based on previous studies (42); *tirasemtiv* dissolved in 1% dimethylsulfoxide). Note that

1% dimethylsulfoxide did not affect muscle fiber contractility (data not shown). After completion of the experiments, the MHC composition of the fibers was determined as described above.

### Effect of *tirasemtiv* on murine muscle fiber types

*Tirasemtiv* is a fast skeletal muscle troponin activator, but the effect of *tirasemtiv* on individual murine type 2A, 2X and 2B fast muscle fibers is not known. Thus, to test the effect of *tirasemtiv* on the various muscle fiber types in mouse muscles, individual fibers were isolated from EDL and permeabilized as described above. The contractility of the permeabilized fibers was determined in the presence/absence of 10 μM *tirasemtiv* (protocol as described above). After completion of the experiments, the MHC isoform composition of the fibers was determined. The resolution of our SDS-PAGE allowed for identification of type 1 and 2B MHC isoforms; type 2A and 2X isoforms appeared as one band and these fibers were therefore grouped.

### Statistics

Data are presented as mean ± standard error of the mean. For statistical analyses, one-way ANOVA's, two-way ANOVA's with Sidak's multiple comparison tests and two-tailed *t* tests were used. A probability value $< 0.05$ was considered statistically significant.

## Supplementary Material

Supplementary Material is available at *HMG* online.

*Conflict of Interest statement*. D.T.H. and F.I.M. are employees of Cytokinetics and were financially compensated for their work.

## Funding

The ERA-NET E-Rare2 grant TREAT-NEMMYOP to C.A.C.O., J.G. and R.B.; and VIDI grant (016.126.319) from the Dutch Organization for Scientific Research to C.A.C.O. A.H.B. was funded by MDA602235 from the Muscular Dystrophy Association USA and generous support for therapy development from the Anderson Family Foundation. *ACTA1*$^{H40Y}$ patient genotyping utilized the resources of the Boston Children's Hospital IDDRC Molecular Genetics Core Laboratory funded by NIH U54HD090255.

## References

1. Jungbluth, H., Treves, S., Zorzato, F., Sarkozy, A., Ochala, J., Sewry, C., Phadke, R., Gautel, M. and Muntoni, F. (2018) Congenital myopathies: disorders of excitation-contraction coupling and muscle contraction. Congenital myopathies: disorders of excitation-contraction coupling and muscle contraction. *Nat. Rev. Neurol.*, **14**, 151–167.
2. Wallgren-Pettersson, C., Sewry, C.A., Nowak, K.J. and Laing, N.G. (2011) Nemaline myopathies. *Semin. Pediatr. Neurol.*, **18**, 230–238.
3. Colombo, I., Scoto, M., Manzur, A.Y., Robb, S.A., Maggi, L., Gowda, V., Cullup, T., Yau, M., Phadke, R., Sewry, C., Jungbluth, H. and Muntoni, F. (2015) Congenital myopathies: natural history of a large pediatric cohort. *Neurology*, **84**, 28–35.
4. Ilkovski, B., Cooper, S.T., Nowak, K., Ryan, M.M., Yang, N., Schnell, C., Durling, H.J., Roddick, L.G., Wilkinson, I., Kornberg, A.J. *et al.* (2001) Nemaline myopathy caused by mutations in the muscle alpha-skeletal-actin gene. *Am. J. Hum. Genet.*, **68**, 1333–1343.
5. Donner, K., Ollikainen, M., Ridanpää, M., Christen, H.J., Goebel, H.H., de Visser, M., Pelin, K. and Wallgren-Pettersson, C. (2002) Mutations in the $\beta$-tropomyosin (TPM2) gene—a rare cause of nemaline myopathy. *Neuromuscul. Disord.*, **12**, 151–158.
6. Laing, N.G., Wilton, S.D., Akkari, P.A., Dorosz, S., Boundy, K., Kneebone, C., Blumbergs, P., White, S., Watkins, H., Love, D.R. and Haan, E. (1995) A mutation in the alpha tropomyosin gene TPM3 associated with autosomal dominant nemaline myopathy. *Nat. Genet.*, **9**, 75–79.
7. Pelin, K., Hilpela, P., Donner, K., Sewry, C., Akkari, P.A., Wilton, S.D., Wattanasirichaigoon, D., Bang, M.L., Centner, T., Hanefeld, F. *et al.* (1999) Mutations in the nebulin gene associated with autosomal recessive nemaline myopathy. *Proc. Natl. Acad. Sci.*, **96**, 2305–2310.
8. Yuen, M., Sandaradura, S.A., Dowling, J.J., Kostyukova, A.S., Moroz, N., Quinlan, K.G., Lehtokari, V.L., Ravenscroft, G., Todd, E.J., Ceyhan-Birsoy, O. *et al.* (2014) Leiomodin-3 dysfunction results in thin filament disorganization and nemaline myopathy. *J. Clin. Invest.*, **124**, 4693–4708.
9. Johnston, J.J., Kelley, R.I., Crawford, T.O., Morton, D.H., Agarwala, R., Koch, T., Schäffer, A.A., Francomano, C.A. and Biesecker, L.G. (2000) A novel nemaline myopathy in the Amish caused by a mutation in troponin T1. *Am. J. Hum. Genet.*, **67**, 814–821.
10. Sandaradura, S.A., Bournazos, A., Mallawaarachchi, A., Cummings, B.B., Waddell, L.B., Jones, K.J., Troedson, C., Sudarsanam, A., Nash, B.M., Peters, G.B. *et al.* (2018) Nemaline myopathy and distal arthrogryposis associated with an autosomal recessive TNNT3 splice variant. *Hum. Mutat.*, **39**, 383–388.
11. Agrawal, P.B., Greenleaf, R.S., Tomczak, K.K., Lehtokari, V.L., Wallgren-Pettersson, C., Wallefeld, W., Laing, N.G., Darras, B.T., Maciver, S.K., Dormitzer, P.R. and Beggs, A.H. (2007) Nemaline myopathy with minicores caused by mutation of the CFL2 gene encoding the skeletal muscle actin-binding protein, cofilin-2. *Am. J. Hum. Genet.*, **80**, 162–167.
12. Miyatake, S., Mitsuhashi, S., Hayashi, Y.K., Purevjav, E., Nishikawa, A., Koshimizu, E., Suzuki, M., Yatabe, K., Tanaka, Y., Ogata, K. *et al.* (2017) Biallelic mutations in MYPN, encoding Myopalladin, are associated with childhood-onset, slowly progressive nemaline myopathy. *Am. J. Hum. Genet.*, **100**, 169–178.
13. Ravenscroft, G., Miyatake, S., Lehtokari, V.-L., Todd, E.J., Vornanen, P., Yau, K.S., Hayashi, Y.K., Miyake, N., Tsurusaki, Y., Doi, H. *et al.* (2013) Mutations in KLHL40 are a frequent cause of severe autosomal-recessive nemaline myopathy. *Am. J. Hum. Genet.*, **93**, 6–18.
14. Gupta, V.A., Ravenscroft, G., Shaheen, R., Todd, E.J., Swanson, L.C., Shiina, M., Ogata, K., Hsu, C., Clarke, N.F., Darras, B.T. *et al.* (2013) Identification of KLHL41 mutations implicates BTB-Kelch-mediated ubiquitination as an alternate pathway to myofibrillar disruption in nemaline myopathy. *Am. J. Hum. Genet.*, **93**, 1108–1117.
15. Sambuughin, N., Yau, K.S., Olivé, M., Duff, R.M., Bayarsaikhan, M., Lu, S., Gonzalez-Mera, L., Sivadorai, P., Nowak, K.J., Ravenscroft, G. *et al.* (2010) Dominant mutations in KBTBD13, a member of the BTB/Kelch family, cause nemaline myopathy with cores. *Am. J. Hum. Genet.*, **87**, 842–847.

16. de Winter, J.M. and Ottenheijm, C.A.C. (2017) Sarcomere dysfunction in nemaline myopathy. *J. Neuromuscul. Dis.*, **4**, 99–113.
17. Ottenheijm, C.A.C., Hooijman, P., DeChene, E.T., Stienen, G.J., Beggs, A.H. and Granzier, H. (2010) Altered myofilament function depresses force generation in patients with nebulin-based nemaline myopathy (NEM2). *J. Struct. Biol.*, **170**, 334–343.
18. de Winter, J.M., Joureau, B., Lee, E.-J., Kiss, B., Yuen, M., Gupta, V.A., Pappas, C.T., Gregorio, C.C., Stienen, G.J.M., Edvardsson, S. *et al.* (2016) Mutation-specific effects on thin filament length in thin filament myopathy. *Ann. Neurol.*, **79**, 959–969.
19. Joureau, B., de Winter, J.M., Conijn, S., Bogaards, S.J.P., Kovacevic, I., Kalganov, A., Persson, M., Lindqvist, J., Stienen, G.J.M., Irving, T.C. *et al.* (2018) Dysfunctional sarcomere contractility contributes to muscle weakness in ACTA1-related nemaline myopathy (NEM3). *Ann. Neurol.*, **83**, 269–282.
20. de Winter, J.M., Molenaar, J.P., Yuen, M., van der Pijl, R., Shen, S., Conijn, S., van de Locht, M., Willigenburg, M., Bogaards, S.J.P., van Kleef, E.S.B. *et al.* (2020) KBTBD13 is an actin-binding protein that modulates muscle kinetics. *J. Clin. Invest.*, **130**, 754–767.
21. Ochala, J. (2008) Thin filament proteins mutations associated with skeletal myopathies: defective regulation of muscle contraction. *J. Mol. Med. (Berl)*, **86**, 1197–1204.
22. Ochala, J., Ravenscroft, G., McNamara, E., Nowak, K.J. and Iwamoto, H. (2015) X-ray recordings reveal how a human disease-linked skeletal muscle $\alpha$-actin mutation leads to contractile dysfunction. *J. Struct. Biol.*, **192**, 331–335.
23. Ochala, J., Iwamoto, H., Larsson, L. and Yagi, N. (2010) A myopathy-linked tropomyosin mutation severely alters thin filament conformational changes during activation. *Proc. Natl. Acad. Sci.*, **107**, 9807–9812.
24. Russell, A.J., Hartman, J.J., Hinken, A.C., Muci, A.R., Kawas, R., Driscoll, L., Godinez, G., Lee, K.H., Marquez, D., Browne, W.F., IV *et al.* (2012) Activation of fast skeletal muscle troponin as a potential therapeutic approach for treating neuromuscular diseases. *Nat. Med.*, **18**, 452–455.
25. Nguyen, M.-A.T., Joya, J.E., Kee, A.J., Domazetovska, A., Yang, N., Hook, J.W., Lemckert, F.A., Kettle, E., Valova, V.A., Robinson, P.J. *et al.* (2011) Hypertrophy and dietary tyrosine ameliorate the phenotypes of a mouse model of severe nemaline myopathy. *Brain*, **134**, 3516–3529.
26. Lee, E.-J., Kolb, J., Hwee, D.T., Malik, F.I. and Granzier, H.L. (2019) Functional characterization of the intact diaphragm in a nebulin-based nemaline myopathy (NM) model-effects of the fast skeletal muscle troponin activator tirasemtiv. *Int. J. Mol. Sci.*, **20**, 5008.
27. Ochala, J., Lehtokari, V.-L., Iwamoto, H., Li, M., Feng, H.Z., Jin, J.P., Yagi, N., Wallgren-Pettersson, C., Pénisson-Besnier, I. and Larsson, L. (2011) Disrupted myosin cross-bridge cycling kinetics triggers muscle weakness in nebulin-related myopathy. *FASEB J.*, **25**, 1903–1913.
28. Malfatti, E., Lehtokari, V.-L., Böhm, J., de Winter, J.M., Schäffer, U., Estournet, B., Quijano-Roy, S., Monges, S., Lubieniecki, F., Bellance, R. *et al.* (2014) Muscle histopathology in nebulin-related nemaline myopathy: ultrastructural findings correlated to disease severity and genotype. *Acta Neuropathol. Commun.*, **2**, 44.
29. Tonino, P., Pappas, C.T., Hudson, B.D., Labeit, S., Gregorio, C.C. and Granzier, H. (2010) Reduced myofibrillar connectivity and increased Z-disk width in nebulin-deficient skeletal muscle. *J. Cell Sci.*, **123**, 384–391.
30. Jasmin, B.J. and Gardiner, P.F. (1987) Patterns of EMG activity of rat plantaris muscle during swimming and other locomotor activities. *J. Appl. Phys.*, **63**, 713–718.
31. Chamberlain, J.S. (2004) Cachexia in cancer - zeroing in on myosin. Cachexia in cancer—zeroing in on myosin. *N. Engl. J. Med.*, **351**, 2124–2125.
32. Cohen, S., Brault, J.J., Gygi, S.P., Glass, D.J., Valenzuela, D.M., Gartner, C., Latres, E. and Goldberg, A.L. (2009) During muscle atrophy, thick, but not thin, filament components are degraded by MuRF1-dependent ubiquitylation. *J. Cell Biol.*, **185**, 1083–1095.
33. Coirault, C., Guellich, A., Barbry, T., Samuel, J.L., Riou, B. and Lecarpentier, Y. (2007) Oxidative stress of myosin contributes to skeletal muscle dysfunction in rats with chronic heart failure. *Am. J. Physiol. Heart Circ. Physiol.*, **292**, H1009–H1017.
34. Cheng, A.J., Yamada, T., Rassier, D.E., Andersson, D.C., Westerblad, H. and Lanner, J.T. (2016) Reactive oxygen/nitrogen species and contractile function in skeletal muscle during fatigue and recovery. *J. Physiol.*, **594**, 5149–5160.
35. Cheng, A.J., Hwee, D.T., Kim, L.H., Durham, N., Yang, H.T., Hinken, A.C., Kennedy, A.R., Terjung, R.L., Jasper, J.R., Malik, F.I. and Westerblad, H. (2019) Fast skeletal muscle troponin activator CK-2066260 increases fatigue resistance by reducing the energetic cost of muscle contraction. *J. Physiol.*, **597**, 4615–4625.
36. Barclay, C.J., Woledge, R.C. and Curtin, N.A. (2007) Energy turnover for $Ca^{2+}$ cycling in skeletal muscle. *J. Muscle Res. Cell. M.*, **28**, 259–274.
37. Kelly, E., Farrell, M.A. and McElvaney, N.G. (2008) Adult-onset nemaline myopathy presenting as respiratory failure. *Respir. Care*, **53**, 1490–1494.
38. Shahrizaila, N., Kinnear, W.J.M. and Wills, A.J. (2006) Respiratory involvement in inherited primary muscle conditions. Respiratory involvement in inherited primary muscle conditions. *J. Neurol. Neurosurg. Psychiatry*, **77**, 1108–1115.
39. Falgà-Tirado, C., Pérez-Pemán, P., Ordi-Ros, J., Bofill, J.M. and Balcells, E. (1995) Adult onset of nemaline myopathy presenting as respiratory insufficiency. *Respiration*, **62**, 353–354.
40. Hwee, D.T., Kennedy, A., Ryans, J., Russell, A.J., Jia, Z., Hinken, A.C., Morgans, D.J., Malik, F.I. and Jasper, J.R. (2014) Fast skeletal muscle troponin activator tirasemtiv increases muscle function and performance in the B6SJL-SOD1G93A ALS mouse model. *PLoS One*, **9**, e96921.
41. Shefner, J.M., Cudkowicz, M.E., Hardiman, O., Cockroft, B.M., Lee, J.H., Malik, F.I., Meng, L., Rudnicki, S.A., Wolff, A.A., Andrews, J.A. and on behalf of the VITALITY-ALS STUDY GROUP (2019) A phase III trial of tirasemtiv as a potential treatment for amyotrophic lateral sclerosis. *Amyotroph. Lateral Scler. Front. Degener.*, **20**, 584–594.
42. de Winter, J.M., Buck, D., Hidalgo, C., Jasper, J.R., Malik, F.I., Clarke, N.F., Stienen, G.J.M., Lawlor, M.W., Beggs, A.H., Ottenheijm, C.A.C. and Granzier, H. (2013) Troponin activator augments muscle force in nemaline myopathy patients with nebulin mutations. *J. Med. Genet.*, **50**, 383–392.
43. Andrews, J.A., Miller, T.M., Vijayakumar, V., Stoltz, R., James, J.K., Meng, L., Wolff, A.A. and Malik, F.I. (2018) CK-2127107 amplifies skeletal muscle response to nerve activation in humans. *Muscle Nerve*, **57**, 729–734.
44. Hwee, D.T., Cheng, A.J., Hartman, J.J., Hinken, A.C., Lee, K., Durham, N., Russell, A.J., Malik, F.I., Westerblad, H. and Jasper,

J.R. (2017) The $Ca^{2+}$ sensitizer CK-2066260 increases myofibrillar $Ca^{2+}$ sensitivity and submaximal force selectively in fast skeletal muscle. *J. Physiol.*, **595**, 1657–1670.
45. Manders, E., Bonta, P.I., Kloek, J.J., Symersky, P., Bogaard, H.J., Hooijman, P.E., Jasper, J.R., Malik, F.I., Stienen, G.J.M., Vonk-Noordegraaf, A., de Man, F.S. and Ottenheijm, C.A.C. (2016) Reduced force of diaphragm muscle fibers in patients with chronic thromboembolic pulmonary hypertension. *Am. J. Physiol. Lung Cell. Mol. Physiol.*, **311**, L20–L28.
46. de Winter, J.M., Joureau, B., Sequeira, V., Clarke, N.F., van der Velden, J., Stienen, G.J.M., Granzier, H., Beggs, A.H. and Ottenheijm, C.A.C. (2015) Effect of levosimendan on the contractility of muscle fibers from nemaline myopathy patients with mutations in the nebulin gene. *Skelet. Muscle*, **5**, 12.
47. Gineste, C., le Fur, Y., Vilmen, C., le Troter, A., Pecchi, E., Cozzone, P.J., Hardeman, E.C., Bendahan, D. and Gondin, J. (2013) Combined MRI and $^{31}$P-MRS investigations of the ACTA1(H40Y) mouse model of nemaline myopathy show impaired muscle function and altered energy metabolism. *PLoS One*, **8**, e61517.
48. Chan, C., Fan, J., Messer, A.E., Marston, S.B., Iwamoto, H. and Ochala, J. (2016) Myopathy-inducing mutation H40Y in ACTA1 hampers actin filament structure and function. *Biochim. Biophys. Acta-Mol. Basis Dis.*, **1862**, 1453–1458.
49. de Man, F.S., van Hees, H.W.H., Handoko, M.L., Niessen, H.W., Schalij, I., Humbert, M., Dorfmüller, P., Mercier, O., Bogaard, H.J., Postmus, P.E. *et al.* (2011) Diaphragm muscle fiber weakness in pulmonary hypertension. *Am. J. Respir. Crit. Care Med.*, **183**, 1411–1418.
50. Gineste, C., de Winter, J.M., Kohl, C., Witt, C.C., Giannesini, B., Brohm, K., le Fur, Y., Gretz, N., Vilmen, C., Pecchi, E. *et al.* (2013) In vivo and in vitro investigations of heterozygous nebulin knock-out mice disclose a mild skeletal muscle phenotype. *Neuromuscul. Disord.*, **23**, 357–369.
51. Moon, R.B. and Richards, J.H. (1973) Determination of intracellular pH by 31P magnetic resonance. *J. Biol. Chem.*, **248**, 7276–7278.
52. Brocca, L., Pellegrino, M.A., Desaphy, J.F., Pierno, S., Camerino, D.C. and Bottinelli, R. (2010) Is oxidative stress a cause or consequence of disuse muscle atrophy in mice? A proteomic approach in hindlimb-unloaded mice: experimental physiology-research paper. *Exp. Physiol.*, **95**, 331–350.
53. Laemmli, U.K. (1970) Cleavage of structural proteins during the assembly of the head of bacteriophage T4. *Nature*, **227**, 680–685.
54. Pellegrino, M.A., Canepari, M., Rossi, R., D'Antona, G., Reggiani, C. and Bottinelli, R. (2003) Orthologous myosin isoform and scaling of shortening velocity with body size in mouse, rat, rabbit and human muscles. Orthologous myosin isoform and scaling of shortening velocity with body size in mouse, rat, rabbit and human muscles. *J. Physiol.*, **546**, 677–689.
55. Cannavino, J., Brocca, L., Sandri, M., Grassi, B., Bottinelli, R. and Pellegrino, M.A. (2015) The role of alterations in mitochondrial dynamics and PGC-1$\alpha$ over-expression in fast muscle atrophy following hindlimb unloading. *J. Physiol.*, **593**, 1981–1995.
56. Agrawal, P.B., Strickland, C.D., Midgett, C., Morales, A., Newburger, D.E., Poulos, M.A., Tomczak, K.K., Ryan, M.M., Iannaccone, S.T., Crawford, T.O., Laing, N.G. and Beggs, A.H. (2004) Heterogeneity of nemaline myopathy cases with skeletal muscle $\alpha$-actin gene mutations. *Ann. Neurol.*, **56**, 86–96.
57. Ottenheijm, C.A.C., Witt, C.C., Stienen, G.J., Labeit, S., Beggs, A.H. and Granzier, H. (2009) Thin filament length dysregulation contributes to muscle weakness in nemaline myopathy patients with nebulin deficiency. *Hum. Mol. Genet.*, **18**, 2359–2369.